Interpericyte tunnelling nanotubes regulate neurovascular coupling

https://doi.org/10.1038/s41586-020-2589-x

Received: 12 December 2018

Accepted: 6 July 2020

Luis Alarcon-Martinez[1,2,4]✉, Deborah Villafranca-Baughman[1,2,4], Heberto Quintero[1,2], J. Benjamin Kacerovsky[3], Florence Dotigny[1,2], Keith K. Murai[3], Alexandre Prat[1,2], Pierre Drapeau[1,2] & Adriana Di Polo[1,2]✉

Signalling between cells of the neurovascular unit, or neurovascular coupling, is essential to match local blood flow with neuronal activity. Pericytes interact with endothelial cells and extend processes that wrap capillaries, covering up to 90% of their surface area[1,2]. Pericytes are candidates to regulate microcirculatory blood flow because they are strategically positioned along capillaries, contain contractile proteins and respond rapidly to neuronal stimulation[3,4], but whether they synchronize microvascular dynamics and neurovascular coupling within a capillary network was unknown. Here we identify nanotube-like processes that connect two bona fide pericytes on separate capillary systems, forming a functional network in the mouse retina, which we named interpericyte tunnelling nanotubes (IP-TNTs). We provide evidence that these (i) have an open-ended proximal side and a closed-ended terminal (end-foot) that connects with distal pericyte processes via gap junctions, (ii) carry organelles including mitochondria, which can travel along these processes, and (iii) serve as a conduit for intercellular Ca^{2+} waves, thus mediating communication between pericytes. Using two-photon microscope live imaging, we demonstrate that retinal pericytes rely on IP-TNTs to control local neurovascular coupling and coordinate light-evoked responses between adjacent capillaries. IP-TNT damage following ablation or ischaemia disrupts intercellular Ca^{2+} waves, impairing blood flow regulation and neurovascular coupling. Notably, pharmacological blockade of Ca^{2+} influx preserves IP-TNTs, rescues light-evoked capillary responses and restores blood flow after reperfusion. Our study thus defines IP-TNTs and characterizes their critical role in regulating neurovascular coupling in the living retina under both physiological and pathological conditions.

Pericytes embedded along capillary walls regulate microcirculatory blood flow by contracting and relaxing to induce changes in capillary diameter[4,5]. This model explains capillary dynamics, but does not account for the need to coordinate dilation and constriction in distal capillaries to achieve fine regulation of blood supply within a local network. Examination of retinas from mice that express red fluorescent protein under control of the NG2 (*Cspg4*) promoter (NG2–DsRed), which allows the selective visualization of retinal pericytes[6], revealed fine processes connecting neighbouring capillaries (Fig. 1a), reminiscent of intervascular bridging strands described in fixed tissue[7–13]. The colocalization of DsRed and TRITC-lectin, which labels both the pericyte's basement membrane and endothelial cells, showed that these processes emerged from the pericyte soma and extended to distal capillaries (Fig. 1b, c). These pericyte-derived structures were tubular (Supplementary Video 1), with an average diameter of 500 nm (Fig. 1d), resembling thin tunnelling nanotubes[14]. They ranged in length from 4 to 90 μm, with a bimodal length distribution; we classified them as either short or long (shorter or longer than 30 μm), and found that short processes were more prevalent than long processes (66% and 34%, respectively) (Fig. 1e, f). Retinal labelling with phalloidin, which binds F-actin, revealed that these pericyte-derived processes contain an F-actin cytoskeleton (Fig. 1g, h), a structural requirement of thin tunnelling nanotubes.

An important phenotypic criterion of thin tunnelling nanotubes is that they connect two distinct cells[14]. Analysis of retinas from NG2–DsRed mice revealed that the pericyte elaborating each thin tunnelling nanotube, referred to here as the proximal pericyte, connected with the process of a pericyte on a distal capillary, thus termed the distal pericyte (Extended Data Fig. 1a–d). We therefore named these processes interpericyte tunnelling nanotubes (IP-TNTs). To investigate whether these structures generally connect two pericytes, we performed single-pericyte electroporation of fluorescein, a low-molecular-weight dye (332 Da). Fluorescein diffused rapidly from the soma of the proximal pericyte into the IP-TNT and, critically, into

---

[1]Department of Neuroscience, University of Montreal, Montreal, Quebec, Canada. [2]University of Montreal Hospital Research Centre, Montreal, Quebec, Canada. [3]Centre for Research in Neuroscience, Department of Neurology and Neurosurgery, The Research Institute of the McGill University Health Centre, Montreal General Hospital, Montreal, Quebec, Canada. [4]These authors contributed equally: Luis Alarcon-Martinez, Deborah Villafranca-Baughman. ✉e-mail: lalarcon@um.es; adriana.di.polo@umontreal.ca

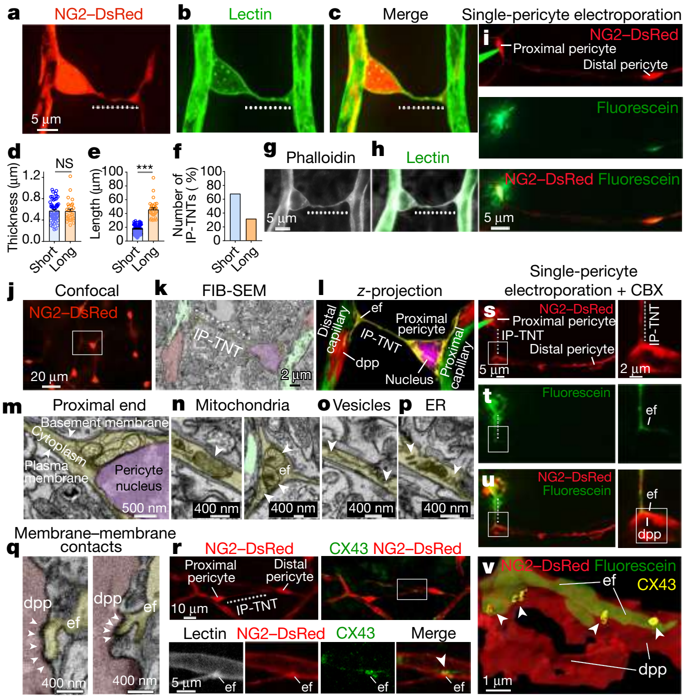

Fig. 1 | IP-TNTs connect pericytes on distal capillaries in a soma-to-process configuration. **a**–**c**, Pericyte extending a nanotube process, which we name an IP-TNT (dotted line), across an adjacent capillary. All retinas presented IP-TNTs. **d**, **e**, IP-TNT diameter ($n = 86$ IP-TNTs/pericytes, $n = 3$ mice; two-tailed Student's *t*-test, NS, not significant) and length ($n = 91$ IP-TNTs/pericytes, $n = 3$ mice; two-tailed Mann–Whitney *U* test, ***$P < 0.001$); data are mean ± s.e.m. **f**, Incidence of short versus long IP-TNTs ($n = 91$ IP-TNTs/pericytes, $n = 3$ mice). **g**, **h**, Labelling of IP-TNTs with phalloidin (**g**) and lectin (**h**), showing F-actin cytoskeleton. **i**, Fluorescein electroporated into a pericyte with IP-TNT diffuses from soma and IP-TNT into distal pericyte (pipette in green; replicated five times). **j**, Pericyte with IP-TNT (inset), visualized by confocal imaging, is selected for FIB-SEM. **k**, Montage of FIB-SEM images of the pericyte in **j** (inset) highlighting its nucleus (purple), IP-TNT (yellow, dotted line), distal pericyte processes (dpp, red) and capillaries (green). **l**, Reconstruction of FIB-SEM images in **k**. **m**, Open-ended side of IP-TNT is continuous with the pericyte cytoplasm. **n**, Mitochondria within IP-TNT (left) and at its end-foot (ef; right). **o**–**q**, IP-TNTs contain vesicles (**o**) and endoplasmic reticulum (ER; **p**), and membrane-to-membrane contacts exist between the IP-TNT ef (yellow) and dpp (red) (**q**). Four hundred FIB-SEM sections of an IP-TNT were analysed. **r**, Top, CX43 immunostaining (green) in two IP-TNT-connected pericytes. Bottom, inset shows CX43 labelling (green) between the IP-TNT ef and the dpp. **s**–**u**, Fluorescein electroporated in the presence of carbenoxolone accumulates in proximal pericyte and IP-TNT (**s**, **t**, left), delineating contact between IP-TNT ef (green) and dpp (red) (**u**). Right, higher magnification of inset (boxed in **s**–**u**). **v**, Higher magnification of inset (boxed in **u**, right) shows localization of CX43-positive plaques (yellow) at interface between IP-TNT ef (green) and dpp (red) (replicated 12 times). The same IP-TNT-coupled pericytes in **s**–**u** were processed for CX43 labelling (replicated three times).

the soma of the distal pericyte (Fig. 1i). In a complementary experiment, we electroporated a form of dextran (3,000 Da) coupled to fluorescein that diffuses well within cells but does not permeate through connexin pores[15]. Our data show that dextran entered the proximal pericyte and its IP-TNT but did not diffuse into the distal pericyte, suggesting that gap junctions are present at this interface. Accumulation of dextran in the proximal pericyte allowed clear identification of the connection between the IP-TNT terminal (end-foot) and the distal pericyte process (Extended Data Fig. 1e, f). We did not detect the electroporated dyes in endothelial cells, and a lack of endothelial cell markers confirmed that IP-TNTs derived uniquely from pericytes (Extended Data Fig. 2a, b).

Correlative serial block-face focused ion-beam scanning electron microscopy (FIB-SEM) revealed that IP-TNTs connect pericytes in a soma-to-process configuration (Fig. 1j–l). In contrast to the multiple thin tunnelling nanotubes described in vitro[16], we found that each IP-TNT is a single process (Fig. 1k, m–p) with a diameter of 487 ± 35 nm, consistent with the calibre estimated from fluorescence imaging (Fig. 1d). IP-TNTs have an open-ended side continuous with the proximal pericyte soma (Fig. 1k–m) and a closed-ended terminal, the end-foot, that connects with the distal pericyte process (Fig. 1k, l, q). IP-TNTs contain a cytoplasm as well as plasma and basement membranes that extend from the proximal pericyte (Fig. 1m). Labelling to detect laminin, a component of the basal lamina, confirmed that IP-TNTs are enclosed by a basement membrane (Extended Data Fig. 2c). Cytoplasmic components identified within IP-TNTs included mitochondria (Fig. 1n), vesicles (Fig. 1o) and endoplasmic reticulum (Fig. 1p), suggestive of local ATP production and vesicle trafficking. Our data showed that IP-TNT end-feet connect with distal pericyte processes through direct membrane-to-membrane contacts, again evocative of gap junctions (Fig. 1q, Supplementary Video 2). Consistent with this, we detected expression of connexin 43 (CX43, also known as GJA1) at IP-TNT end-feet both by immunolabelling and in CX43–ECFP reporter mice[17] (Fig. 1r, Extended Data Fig. 2d). When fluorescein was electroporated into the proximal pericyte in the presence of the gap junction blocker carbenoxolone, it accumulated in the soma and IP-TNT, delineating the connection with the distal pericyte (Fig. 1s–u). Immunohistochemical labelling of CX43 in the same electroporated retinas showed CX43-positive plaques at the interface between the IP-TNT end-foot and the distal pericyte process (Fig. 1v). Collectively, these findings indicate that two bona fide pericytes connect via IP-TNTs and communicate through CX43-based gap junctions.

Retinal capillary pericytes contain α-SMA, a protein essential for pericyte contractility[3]. Similarly, IP-TNTs also contain α-SMA (Extended Data Fig. 2e), suggesting the presence of a contractile apparatus. By contrast, we did not detect expression of α-tubulin in IP-TNTs (Extended Data Fig. 2f). IP-TNTs also contained focal adhesion kinase 1 (FAK) and ribosomal protein S6 (Extended Data Fig. 2g, h), but not growth-associated protein 43 (GAP43) or markers of mesenchymal stem cells (Extended Data Fig. 2i–l), suggesting that these structures lack stem-cell-like properties. Besides the retina, we also detected IP-TNTs in the visual cortex (Extended Data Fig. 2m, n). We found that IP-TNTs were abundant in all vascular plexuses (51.4 ± 3.4 IP-TNTs per mm^2) and in 28% of NG2–positive retinal pericytes (Extended Data Fig. 3a, b), with a higher density in the deep and intermediate plexuses (22.4 ± 1.6 and 20.5 ± 1.8 IP-TNTs per mm^2, respectively) than in the superficial bed (9.0 ± 0.9 IP-TNTs per mm^2). Most capillaries connected by IP-TNTs (87%) originated from different branches (Extended Data Fig. 3c, d). IP-TNTs connected capillaries of either the same or different order relative to the upstream arteriole (first order), mostly fourth- to eighth-order vessels (Extended Data Fig. 3e, f).

To investigate IP-TNT function in vivo, we performed non-invasive live visualization of the retina with two-photon laser-scanning microscopy (TPLSM) (Fig. 2a). The resulting high-resolution images of a network of IP-TNTs linking distal capillaries provided the first evidence, to our knowledge, of these processes in living mice (Fig. 2b–d). Using TPLSM, we found that IP-TNTs also contain an F-actin cytoskeleton in vivo (Fig. 2e). Thin tunnelling nanotubes that contain F-actin can shuttle organelles, including mitochondria[18]. Analysis of mito-Dendra2 mice, which allow visualization of mitochondria[19], confirmed that mitochondria were present in IP-TNTs and travelled along them in living retinas (Fig. 2f). However, mitochondrial transport between pericytes was not observed, consistent with the closed-ended nature of IP-TNTs (Fig. 1k, l, q).

TNT-like structures can mediate cell-to-cell communication through intercellular Ca^{2+} waves[20]. To investigate whether these waves propagate along IP-TNTs, we imaged retinal pericytes by TPLSM in mice expressing GCaMP6, a Ca^{2+} indicator, under the control of the NG2 promoter

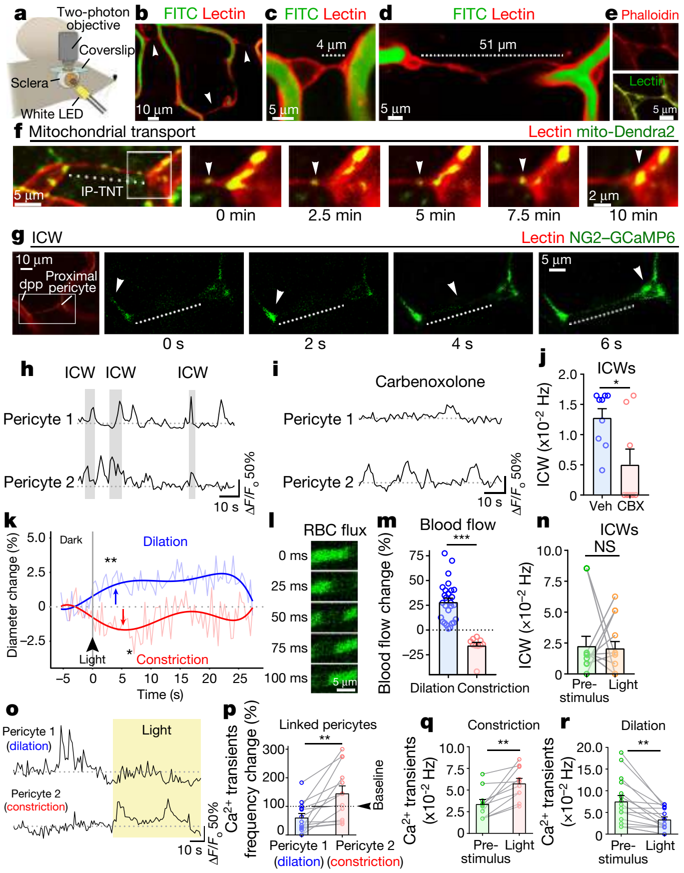

Fig. 2 | IP-TNTs are a conduit for pericyte-to-pericyte communication in living retinas. a, Setup for two-photon laser scanning microscopy (TPLSM). **b**, In vivo imaging using intravenously applied FITC (to visualize capillaries) and intravitreally injected lectin (to label the basement membrane of pericytes) shows a network of IP-TNTs linking distal capillaries, observed in all retinas analysed. **c**, **d**, Short and long IP-TNTs exist in all vascular plexuses. **e**, Colabelling with phalloidin to detect F-actin (top) and lectin to visualize pericytes/IP-TNTs (bottom) shows that IP-TNTs contain an F-actin cytoskeleton. **f**, Time-lapse imaging shows mitochondria travelling within an IP-TNT (arrow; replicated 3 times). **g**, TPLSM recordings show intercellular Ca^{2+} wave (ICWs) propagating through an IP-TNT (dotted line; replicated in 57 IP-TNTs, $n = 20$ mice). **h**, ICWs are synchronous Ca^{2+} increases in IP-TNT-coupled pericyte pairs (grey). **i**, **j**, ICW frequency decreases with carbenoxolone (CBX) treatment (in **j**, vehicle: $n = 18$ capillaries, $n = 4$ mice; CBX: $n = 16$ capillaries, $n = 4$ mice; $^*P = 0.029$). **k**, Longitudinal analysis of light-evoked changes in capillary diameter in vivo (blue, dilation, $n = 39$ capillaries, $n = 2$ mice; red, constriction, $n = 30$ capillaries, $n = 2$ mice; $^*P < 0.05$, $^{**}P < 0.01$). **l**, TPLSM quantification of red blood cells (RBC) per time unit after light stimulation (replicated in 224 capillaries, $n = 28$ mice). **m**, IP-TNT-linked capillaries undergo opposite blood flow responses (dilation: $n = 27$ capillaries, $n = 2$ mice; constriction: $n = 10$ capillaries, $n = 2$ mice; $^{***}P < 0.001$). **n**, ICWs in IP-TNT-linked capillaries before and after light stimulation ($n = 13$ capillaries per group, $n = 5$ mice per group; NS, not significant). **o**, **p**, A decrease in Ca^{2+} transient frequency correlates with dilation (pericyte 1), whereas increased frequency correlates with constriction in the coupled pericyte (pericyte 2). **p** shows Ca^{2+} transient frequency changes in IP-TNT-linked pericytes ($n = 13$ pericytes per group, $n = 5$ mice per group; $^{**}P < 0.01$). **q**, **r**, Pericytes at constricting and dilating capillaries display increases and decreases in Ca^{2+} transient frequency, respectively (constriction: $n = 10$ pericytes, $n = 5$ mice; dilation: $n = 16$ pericytes, $n = 5$ mice, $^{**}P = 0.008$). Data are mean ± s.e.m. **j**, **m**, **n**, two-tailed Mann–Whitney *U* test; **k**, two-tailed ANOVA Dunnett's test; **p**–**r**, two-tailed Student's *t*-test.

(NG2–GCaMP6). Intercellular Ca^{2+} waves, measured as spontaneous synchronous Ca^{2+} increases in IP-TNT-coupled pericytes, propagated bidirectionally along IP-TNTs (Fig. 2g, h, Extended Data Fig. 4, Supplementary Videos 3 and 4). Wave frequency decreased after administration of carbenoxolone (Fig. 2i, j), consistent with our observation that IP-TNTs connect with distal pericyte processes via gap junctions, a prerequisite for the propagation of these waves[21].

To determine whether IP-TNTs contribute to the microvascular response downstream of neuronal activity, we characterized capillary dynamics by TPLSM upon light stimulation of the retina (Extended Data Fig. 5a). Capillaries displayed little change in diameter or spontaneous activity before the light stimulus was administered (Extended Data Fig. 5b). By contrast, light triggered the constriction of some vessels (57%) and the dilation of others (43%) (Fig. 2k, Extended Data Fig. 5c, d). Notably, capillary pairs connected by IP-TNTs always exhibited simultaneous, but opposite, responses concomitant with light stimulation: one capillary dilated while the other constricted. Specifically, when the proximal capillary dilated, the distal capillary constricted, and vice versa. Dilation and constriction became significant at 4 and 7 s after light onset, respectively (Fig. 2k), and returned to baseline at about 25–30 s. Coordinated responses in capillaries linked by IP-TNTs were also observed in retinal explants (Supplementary Video 5) and were substantially faster than changes in arterioles (vessels more than 9 µm in diameter) (Extended Data Fig. 5e–g).

We measured single-capillary blood flow using TPLSM to quantify the number of red blood cells per time unit[22] before and after light stimulation in vivo (Fig. 2l, Supplementary Video 6). Similar to the calibre changes, IP-TNT-linked capillaries underwent matched opposite responses: one capillary dilated to increase blood flow while the other constricted to reduce blood perfusion (Fig. 2m). IP-TNTs were never observed in the choroid, which—unlike the retinal vasculature—is not autoregulated and changes passively depending on arterial blood pressure[23]. Intercellular Ca^{2+} waves continued to oscillate between IP-TNT-linked pericytes after light stimulation (Fig. 2n). In addition, light-evoked capillary dilation and constriction correlated with opposite and synchronized Ca^{2+} transients, including non-intercellular Ca^{2+} waves, in pericytes connected by IP-TNTs (Fig. 2o, p). Indeed, pericytes at constricting capillaries showed an increase in total Ca^{2+} transient frequency, whereas those at dilating capillaries showed a significant reduction (Fig. 2q, r).

To establish the functional role of IP-TNTs in the neurovascular response to light, we performed laser-induced ablation of individual IP-TNTs (Fig. 3a, b). IP-TNT ablation substantially reduced the frequency of intercellular Ca^{2+} waves in coupled pericytes (Fig. 3c–e). Notably, IP-TNT damage also eliminated the ability of linked capillaries to undergo coordinated dilation and constriction elicited by light (Fig. 3f, g). Before ablation, IP-TNT-connected capillary pairs readily dilated and constricted upon light stimulation, but destruction of IP-TNTs completely impaired these coordinated light-evoked diameter changes (Fig. 3h). Furthermore, IP-TNT damage severely compromised the ability of the capillaries to regulate blood flow in response to neuronal activity (Fig. 3i). The laser parameters used here did not injure endothelial cells or alter blood retinal barrier integrity (Extended Data Fig. 6). Moreover, when the same laser parameters were applied to adjacent retinal ganglion cells, as controls, capillary dynamics, Ca^{2+} responses and retinal ganglion cell numbers were maintained (Extended Data Fig. 7). Hence, the laser parameters used for IP-TNT ablation did not cause damage to neighbouring cells and did not account for the loss of haemodynamic responses shown here.

Pericytes have been proposed to constrict capillaries and impair blood flow in conditions such as stroke[2,24]. To investigate the response of IP-TNTs to ischaemic damage, we blocked the central retinal artery to transiently interrupt blood flow to the retina (Fig. 4a). TPLSM imaging revealed a significant reduction in capillary diameter at pericyte locations (Fig. 4b, c). This reduction was not due to fluorescence bleaching of trapped dextran particles (Extended Data Fig. 8a, b). Post hoc analysis further confirmed that constricted capillaries were much more prevalent in ischaemic retinas than in sham-treated controls

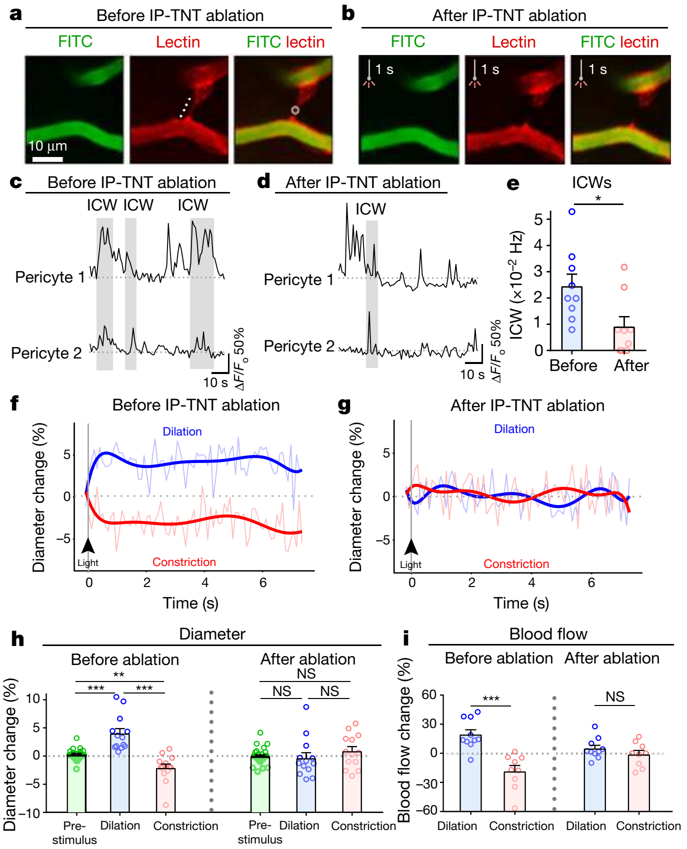

Fig. 3 | IP-TNT ablation disrupts haemodynamic responses and neurovascular coupling. **a**, **b**, IP-TNT before (**a**) and after (**b**) laser ablation (white circle; replicated in 22 IP-TNTs, $n = 10$ mice). **c**, **d**, Ca^{2+} transients in two IP-TNT-connected pericytes before (**c**) and after IP-TNT damage (**d**) show marked decrease in ICWs (grey). **e**, IP-TNT ablation reduces ICWs frequency in coupled pericytes ($n = 18$ capillaries per group, $n = 4$ mice per group; $^{*}P = 0.02$). **f**, **g**, IP-TNT damage eliminates the ability of coupled capillaries to dilate (blue) and constrict (red) with light (arrow; $n = 13$ capillaries per group). **h**, IP-TNT damage impairs light-evoked capillary dilation and constriction (pre-stimulus: $n = 30$ capillaries, $n = 6$ mice; dilation: $n = 13$ capillaries, $n = 6$ mice; constriction: $n = 13$ capillaries, $n = 6$ mice; $^{**}P < 0.01$, $^{***}P < 0.001$, NS, not significant). **i**, Light-dependent blood flow regulation is compromised after IP-TNT ablation (dilation: $n = 20$ capillaries, $n = 3$ mice; constriction: $n = 18$ capillaries, $n = 3$ mice; $^{***}P < 0.001$, NS, not significant). Data are mean ± s.e.m. **e**, **i**, two-tailed Student's *t*-test; **h**, two-tailed ANOVA Tukey's test.

(Extended Data Fig. 8c, d). The diameter of larger vessels did not change (Extended Data Fig. 8e), indicating that this difference was not caused by changes in upstream vessels.

Ischaemia damaged a substantial number of IP-TNTs both in vivo and ex vivo (Fig. 4d, e, Supplementary Video 7). We observed a tenfold increase in ruptured IP-TNTs in ischaemic retinas relative to sham-operated controls, accounting for 22% of all IP-TNTs (total non-injured: 51.4 ± 3.4 IP-TNTs per mm^2; ischaemia: 11.3 ± 3.3 ruptured IP-TNTs per mm^2; sham: 1.1 ± 0.5 ruptured IP-TNTs per mm^2) (Fig. 4f). IP-TNT breakage also occurred in retinal explants subjected to oxygen–glucose deprivation to mimic ischaemia (Extended Data Fig. 8f–h). By contrast, in sham-operated control retinas, IP-TNTs were stable and did not change even over prolonged imaging periods (Fig. 4f). To determine whether IP-TNT damage affected neurovascular coupling, we investigated microvessel dynamics and associated blood flow during ischaemia and reperfusion after reopening of the ophthalmic artery. IP-TNT breakage was accompanied by a substantial loss of light-evoked capillary responses, notably impaired dilation, as well as an inability to regulate blood flow after reperfusion (Fig. 4g–i). These changes could

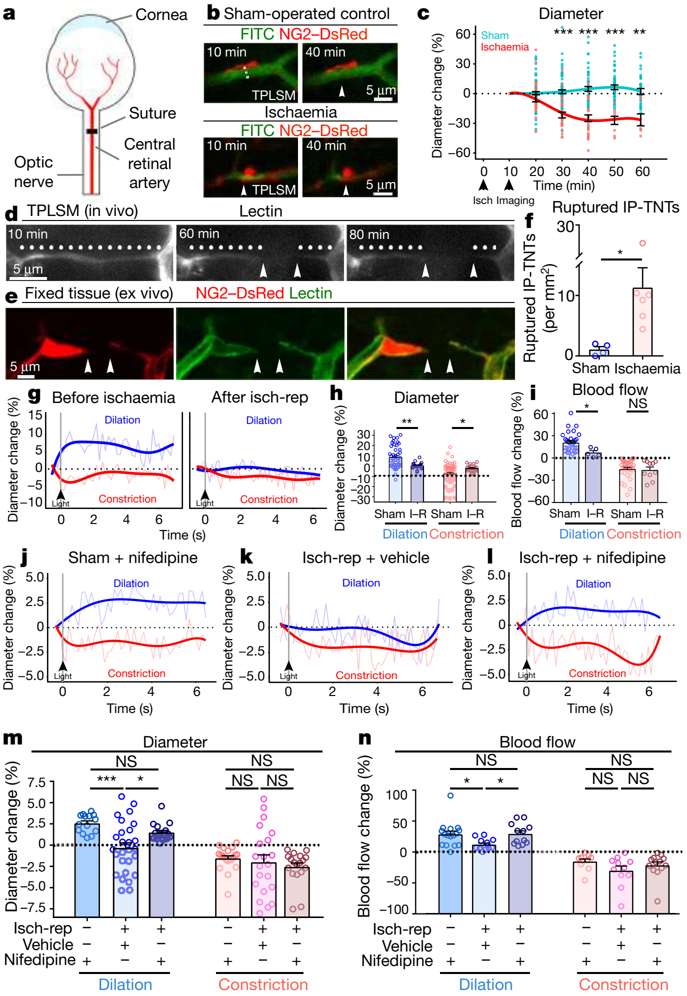

Fig. 4 | Ischaemia damages IP-TNTs and leads to microvascular dysfunction. **a**, Retinal ischaemia induced by transient ligature of ophthalmic vessels. **b**, TPLSM imaging of pericytes and capillaries at 10 and 40 min after induction of ischaemia or sham surgery (replicated 3 times per group). **c**, TPLSM shows reduction in capillary diameter in ischaemia relative to sham controls (sham: $n = 75$ capillaries, $n = 3$ mice; ischaemia: $n = 29$ capillaries, $n = 3$ mice; $^{**}P < 0.01$, $^{***}P < 0.001$). **d**, Time-lapse TPLSM imaging of IP-TNT (dotted line) disintegration during ischaemia (arrows; replicated 3 times). **e**, Ischaemia also ruptures IP-TNTs ex vivo. **f**, Increase in damaged IP-TNTs in ischaemia relative to controls (ischaemia: $n = 6$ mice; sham-operated: $n = 4$; $^{*}P = 0.038$). **g**–**i**, IP-TNT damage induced by ischaemia–reperfusion causes loss of light-evoked capillary dilation (blue) and constriction (red) (pre-ischaemia: dilation, $n = 21$ capillaries, $n = 3$ mice, constriction, $n = 21$ capillaries, $n = 3$ mice; post-ischaemia: dilation, $n = 18$ capillaries, $n = 4$ mice, constriction, $n = 21$ capillaries, $n = 5$ mice). **h**, Capillary responses are impaired in ischaemia (dilation: sham, $n = 46$ capillaries, $n = 3$ mice, ischaemia–reperfusion (I–R), $n = 20$, $n = 4$ mice; constriction: sham, $n = 60$, $n = 3$ mice, reperfusion, $n = 21$, $n = 5$ mice; $^{*}P = 0.016$, $^{**}P = 0.002$). **i**, Blood flow is compromised in ischaemia–reperfusion (dilation: sham, $n = 31$ capillaries, $n = 5$ mice, reperfusion, $n = 5$ capillaries, $n = 5$ mice; constriction: sham, $n = 28$ capillaries, $n = 5$ mice, reperfusion, $n = 10$ capillaries, $n = 5$ mice; $^{*}P = 0.034$, NS, not significant). **j**–**m**, Nifedipine restores light-evoked capillary responses (dilation: sham + nifedipine, $n = 14$ capillaries, $n = 4$, reperfusion + vehicle, $n = 27$ capillaries, $n = 5$, reperfusion + nifedipine, $n = 17$ capillaries, $n = 4$; constriction: sham + nifedipine, $n = 20$ capillaries, $n = 4$, reperfusion + vehicle, $n = 21$ capillaries, $n = 5$, reperfusion + nifedipine, $n = 18$ capillaries, $n = 4$; $^{*}P < 0.05$, $^{***}P < 0.001$, NS, not significant). **n**, Blood flow is impaired after ischaemia–reperfusion, but restored by nifedipine (dilation: sham + nifedipine, $n = 16$ capillaries, $n = 4$, reperfusion + vehicle, $n = 13$ capillaries, $n = 5$, reperfusion + nifedipine, $n = 12$ capillaries, $n = 4$; constriction: sham + nifedipine, $n = 10$ capillaries, $n = 4$, reperfusion + vehicle, $n = 11$ capillaries, $n = 5$, reperfusion + nifedipine, $n = 13$ capillaries, $n = 4$; $^{*}P < 0.05$, NS, not significant). Data are mean ± s.e.m. **c**, **m**, **n**, two-tailed ANOVA Tukey's test; **f**, **h**, **i**, two-tailed Student's *t*-test.

not be attributed to pericyte or retinal ganglion cell death because there was no significant loss of these cells after transient ischaemia (Extended Data Fig. 8i, j). Measurement of focal ischaemia generated with a laser pulse aimed at single capillaries after injection of Rose bengal in tail veins[25] (Extended Data Fig. 8k) showed that capillary responses were substantially reduced in ischaemic microregions (150–200 μm) (Extended Data Fig. 8l) and correlated tightly with the loss of IP-TNTs (with 11 ± 3.4 versus 1.2 ± 0.6 ruptured IP-TNTs per mm^2 detected for ischaemic versus non-ischaemic areas, respectively, in the same retinas) (Extended Data Fig. 8m).

To investigate whether alterations in Ca^{2+} homeostasis promoted IP-TNT rupture during ischaemia, we performed TPLSM imaging in NG2–GCaMP6 mice. Ischaemia rapidly induced a robust, sustained increase in global Ca^{2+} in IP-TNT-coupled pericytes (Supplementary Video 8), whereas little or no Ca^{2+} influx was detected in sham-operated controls (Extended Data Fig. 9a–c). Of interest, Ca^{2+} increase during ischaemia markedly reduced the frequency of intercellular Ca^{2+} waves in IP-TNT-connected pericytes (Extended Data Fig. 9d–f). Ca^{2+} influx to pericytes occurs through nifedipine-sensitive L-type voltage-gated Ca^{2+} channels[26], and hence we investigated the effect of nifedipine on IP-TNT integrity and function. A single intraocular injection of nifedipine, just before ischaemia, decreased Ca^{2+} load (Extended Data Fig. 9g, h) and attenuated IP-TNT damage (vehicle: 8.0 ± 1.6 ruptured IP-TNTs/mm^2, nifedipine: 3.0 ± 0.7 ruptured IP-TNTs/mm^2) (Extended Data Fig. 9i). Nifedipine rescued light-evoked capillary responses (Fig. 4j–l), notably dilation (Fig. 4m), and restored blood flow after reperfusion (Fig. 4n). These results indicate that Ca^{2+} homeostasis is critical to preserving IP-TNT structure and function.

In summary, our study identifies and characterizes IP-TNTs, nanotube-like processes that are essential for pericyte-to-pericyte communication and neurovascular coupling in vivo. We present multiple lines of evidence that argue against the idea that IP-TNTs are empty sleeves from regressing vessels or bridging pericytes[13,27], and rather support their similarity to closed-ended thin tunnelling nanotubes. These include (i) lack of endothelial cell markers, (ii) expression of α-SMA, (iii) presence of organelles and transport of mitochondria, (iv) process stability and (v) existence of bidirectional intercellular Ca^{2+} waves. We report that capillary pairs connected by IP-TNTs exhibit opposite responses concomitant with light stimulation: one capillary dilates to increase blood flow, while the other constricts to decrease blood availability. This observation challenges a simplistic model in which light triggers only dilation, hence increasing blood perfusion. Instead, our findings reflect the complex spatial and temporal heterogeneity of blood redistribution within a circumscribed capillary network, in which a limited amount of blood must be rapidly relocated to meet the demand of active versus inactive neurons[28]. Microvascular deficits, particularly in retinal and brain diseases with an ischaemic component, might result from loss of IP-TNTs. Strategies that protect IP-TNTs should be beneficial for restoring neurovascular coupling and microcirculatory blood flow to support coordinated neuronal function.

Online content

Any methods, additional references, Nature Research reporting summaries, source data, extended data, supplementary information, acknowledgements, peer review information; details of author contributions and competing interests; and statements of data and code availability are available at https://doi.org/10.1038/s41586-020-2589-x.

1. Attwell, D., Mishra, A., Hall, C. N., O'Farrell, F. M. & Dalkara, T. What is a pericyte? *J. Cereb. Blood Flow Metab*. **36**, 451–455 (2016).
2. Dalkara, T. & Alarcon-Martinez, L. Cerebral microvascular pericytes and neurogliovascular signaling in health and disease. *Brain Res*. **1623**, 3–17 (2015).
3. Alarcon-Martinez, L. et al. Capillary pericytes express α-smooth muscle actin, which requires prevention of filamentous-actin depolymerization for detection. *eLife* **7**, e34861 (2018).
4. Hall, C. N. et al. Capillary pericytes regulate cerebral blood flow in health and disease. *Nature* **508**, 55–60 (2014).
5. Hamilton, N. B., Attwell, D. & Hall, C. N. Pericyte-mediated regulation of capillary diameter: a component of neurovascular coupling in health and disease. *Front. Neuroenergetics* **2**, 5 (2010).
6. Zhu, X., Bergles, D. E. & Nishiyama, A. NG2 cells generate both oligodendrocytes and gray matter astrocytes. *Development* **135**, 145–157 (2008).
7. Henle, F. Ueber die Ausbreitung des Epithelium im menschlichen Körper. *Arch. Anat. Physiol. Wiss. Med*. **1838**, 103–128 (1838).
8. Cerletti, U. Die gefassvermehrung in zentralnervensystem. *Histol. Histopathol. Arb. Grosshirnr*. **4**, 1–168 (1910).
9. Cammermeyer, J. A comparative study of intervascular connective tissue strands in the central nervous system. *J. Comp. Neurol*. **114**, 189–208 (1960).
10. Reissenweber, N. J. & Pessacq, T. Intervascular strands in the central nervous system. A histochemical approach. *Acta Anat*. **78**, 51–57 (1971).
11. Williamson, J. R., Tilton, R. G., Kilo, C. & Yu, S. Immunofluorescent imaging of capillaries and pericytes in human skeletal muscle and retina. *Microvasc. Res*. **20**, 233–241 (1980).
12. Leibnitz, L. & Bär, B. A blood capillaries-bridging cell type in adult mammalian brains. *J. Hirnforsch*. **29**, 367–375 (1988).
13. Mendes-Jorge, L. et al. Intercapillary bridging cells: immunocytochemical characteristics of cells that connect blood vessels in the retina. *Exp. Eye Res*. **98**, 79–87 (2012).
14. Korenkova, O., Pepe, A. & Zurzolo, C. Fine intercellular connections in development: TNTs, cytonemes, or intercellular bridges? *Cell Stress* **4**, 30–43 (2020).
15. Harris, A. L. Connexin channel permeability to cytoplasmic molecules. *Prog. Biophys. Mol. Biol*. **94**, 120–143 (2007).
16. Sartori-Rupp, A. et al. Correlative cryo-electron microscopy reveals the structure of TNTs in neuronal cells. *Nat. Commun*. **10**, 342 (2019).
17. Theofilas, P., Steinhäuser, C., Theis, M. & Derouiche, A. Morphological study of a connexin 43-GFP reporter mouse highlights glial heterogeneity, amacrine cells, and olfactory ensheathing cells. *J. Neurosci. Res*. **95**, 2182–2194 (2017).
18. Rustom, A., Saffrich, R., Markovic, I., Walther, P. & Gerdes, H.-H. Nanotubular highways for intercellular organelle transport. *Science* **303**, 1007–1010 (2004).
19. Pham, A. H., McCaffery, J. M. & Chan, D. C. Mouse lines with photo-activatable mitochondria to study mitochondrial dynamics. *Genesis* **50**, 833–843 (2012).
20. Osswald, M. et al. Brain tumour cells interconnect to a functional and resistant network. *Nature* **528**, 93–98 (2015).
21. Wang, X., Veruki, M. L., Bukoreshtliev, N. V., Hartveit, E. & Gerdes, H.-H. Animal cells connected by nanotubes can be electrically coupled through interposed gap-junction channels. *Proc. Natl Acad. Sci. USA* **107**, 17194–17199 (2010).
22. Longden, T. A. et al. Capillary K$^+$-sensing initiates retrograde hyperpolarization to increase local cerebral blood flow. *Nat. Neurosci*. **20**, 717–726 (2017).
23. Nilsson, S. F. & Alm, A. in *Ocular Blood Flow* (eds Kiel, J. W. & Schmetterer, L.) 25–47 (Springer-Verlag, 2012).
24. Alarcon-Martinez, L. et al. Retinal ischemia induces α-SMA-mediated capillary pericyte contraction coincident with perivascular glycogen depletion. *Acta Neuropathol. Commun*. **7**, 134 (2019).
25. Underly, R. G. & Shih, A. Y. Photothrombotic induction of capillary ischemia in the mouse cortex during in vivo two-photon imaging. *Bio Protoc*. **7**, e2378 (2017).
26. Borysova, L., Wray, S., Eisner, D. A. & Burdyga, T. How calcium signals in myocytes and pericytes are integrated across in situ microvascular networks and control microvascular tone. *Cell Calcium* **54**, 163–174 (2013).
27. Franco, C. A. et al. Dynamic endothelial cell rearrangements drive developmental vessel regression. *PLoS Biol*. **13**, e1002125 (2015).
28. Yu, D.-Y. et al. Retinal capillary perfusion: spatial and temporal heterogeneity. *Prog. Retin. Eye Res*. **70**, 23–54 (2019).

Methods

Experimental animals

Animal procedures were approved by the University of Montreal Hospital Research Centre and followed the Canadian Council on Animal Care guidelines. Experiments included adult female and male mice (2–6 months of age, 20–35 g) expressing (i) red fluorescent protein under control of the NG2 (*Cspg4*) promoter (NG2–DsRed) for selective visualization of retinal pericytes (008241, Jackson Laboratory), (ii) the Ca^{2+} indicator GCaMP6 (fast kinetics) downstream of the NG2 promoter (NG2-GCaMP6), generated by crossing NG2-Cre mice (008533, Jackson Laboratory) with *lox*P-flanked GCaMP6 mice (024106, Jackson Laboratory), and (iii) dendra2 fluorescent protein in mitochondria of all cells (mito-Dendra2, 018397, Jackson Laboratory). CX43–ECFP reporter mice carrying enhanced cyan fluorescent protein (ECFP) under control of the CX43 promoter[17] were kindly provided by C. Steinhäuser (Institute of Cellular Neurosciences, University of Bonn). For two-photon live imaging, albino mice were generated by backcrossing with CD-1 mice. Animals were housed in 12 h light/12 h dark cyclic light conditions, with an average in-cage illumination level of 10 lx, and fed ad libitum. Ambient temperature and humidity were maintained at 21–22 °C and 45–55%, respectively. All procedures were performed under general anaesthesia (20 mg ketamine, 2 mg xylazine and 0.4 mg acepromazine per kg body weight).

Retinal and brain immunohistochemistry

Mice were deeply anaesthetized and transcardially perfused with 4% paraformaldehyde (PFA) or methanol. Eyes and brains were immediately collected and processed to generate cryosections that were labelled with 488- or 647-nm-coupled lectin (*Bandeiraea simplicifolia*) (5 μg ml^{-1}, Thermo Fisher). Fluorescent phalloidin (200 U ml^{-1}, Biotium) was used to label F-actin. In addition, retinal sections were incubated with the following primary antibodies: CX43 (3.7 μg ml^{-1}, Sigma), VE-cadherin (20 μg ml^{-1}, R&D Systems), CD31 (2 μg ml^{-1}, BD Pharmingen), alpha smooth muscle actin (α-SMA, 10 μg ml^{-1}, Sigma), alpha tubulin (7.5 μg ml^{-1}, Sigma), laminin (2.5 μg ml^{-1}, Sigma), focal adhesion kinase (FAK, 10 μg ml^{-1}, Abcam), S6 ribosomal protein (4 μg ml^{-1}, Cell Signaling), GAP43 (3.4 μg ml^{-1}, Abcam), CD90 (4 μg ml^{-1}, BD Bioscience), CD44 (10 μg ml^{-1}, eBioscience) and CD45 (10 μg ml^{-1}, Biolegend); or were incubated with RNA binding protein with multiple splicing (RBPMS, 1:500, PhosphoSolutions), a marker specific for retinal ganglion cells. Antibodies were incubated in blocking solution (10% goat serum albumin in PBST) at 4 °C overnight, except RBPMS, which was applied for 3 d, followed by fluorophore-conjugated secondary antibodies (2–4 μg ml^{-1}, Invitrogen). Positive controls included postnatal day 5 retinal axons for GAP43, peripheral leukocytes for CD44 and CD45, retinal ganglion cells for CD90 and retinal vessels for endothelial proteins. Single images or *z* stacks for each IP-TNT were acquired using confocal microscopy and, where indicated, 3D reconstruction was done using Imaris software (Bitplane). A minimum of 100 IP-TNT-connected pericytes in five different mice were analysed for each marker.

Plexus and branch order analysis

Plexus and branch order analyses were performed in flat-mounted retinas of NG2–DsRed mice labelled with 488 nm lectin (5 μg ml^{-1}, Sigma) to visualize IP-TNTs. We used an unbiased stereological approach based on systematic uniform random sampling from 3D disectors (stacks) across the entire retina (6 slices with a field of view of 170 × 136 μm along the *z* axis) (Extended Data Fig. 3a). An image of the vasculature within the 3D-disector frame was acquired with an Axio Imager M2 optical sectioning microscope (×40 objective, Zeiss) and analysed using ImageJ (National Institute of Health: NIH). The first-order vessel was defined as the first branch division from the central retinal artery, and subsequent branches were assigned consecutive higher orders. Using this approach, we determined the vessel order of IP-TNT-connected capillaries and whether they emanated from the same or different origin branches. The total number of IP-TNTs was calculated using the fractionator method[29] as follows: total IP-TNT number = IP-TNT number/asf, where asf is an area sampling fraction of 1/9 (asf = [*a*(frame)]/area *x*–*y* step between disectors). This analysis yielded the total number of IP-TNTs throughout the entire retina and in individual plexuses, which was then used to calculate the number of IP-TNTs per mm^2.

IP-TNT characterization

Retinal images were obtained using an Axio Imager M2 optical sectioning microscope (Zeiss) equipped with an automatically-controlled specimen stage for *x*-, *y*- and *z*-axis movement, a colour camera (Axiocam 509 mono, Zeiss), and image analysis software (Zen, Zeiss). A total of 91 IP-TNTs were randomly selected using systematic uniform random sampling, as described above, and *z* stacks were generated and 3D reconstruction performed using Imaris software (Bitplane). For process length assessment, each IP-TNT was measured along the *x*, *y* and *z* planes using the Imaris filament tracing tool (Bitplane). The diameter of each IP-TNT was measured at the middle point between the proximal pericyte soma and the end-foot junction with the distal pericyte.

Single-pericyte electroporation

Retinal explants from NG2–DsRed mice were superfused with oxygenated bicarbonate-buffered artificial cerebrospinal fluid solution (aCSF: 145 mM NaCl, 26 mM $NaHCO_3$, 1.2 mM Na_2HPO_4, 2.5 mM KCl, 1.3 mM $MgCl_2$, 2.5 mM $CaCl_2$, 10 mM glucose, pH 7.4) bubbled with 95% O_2, 5% CO_2 at 34 °C. Single pericytes were electroporated using a patch pipette filled with aCSF and fluorescein (332 Da, 5%, Fluorescite, Novartis Pharma) or fluorescein-coupled dextran (3,000 Da, 1%, Thermo Fisher). For experiments using carbenoxolone (30 μM), retinas were superfused for at least 20 min to ensure adequate tissue penetration of this gap junction blocker. We applied 20 pulses of a 200-Hz electrical pulse at 50–60 V for 100 ms at 1-s intervals. Time-lapse images were acquired using a Quorum Technologies spinning-disk confocal microscope with a CSU10B (Yokogawa) spinning head mounted on an Olympus BX61W1 fluorescence microscope (Olympus) and connected to a Hamamatsu ORCA-ER camera (Hamamatsu Photonics). Images were captured using the Volocity software (Improvision) and analysed with ImageJ (NIH).

Intravitreal injections

The following fluorescent probes or reagents were administered by intravitreal injection (2 μl total volume): TRITC-lectin (5 μg ml^{-1} Sigma), phalloidin (Biotium) (1 μg ml^{-1}), carbenoxolone (30 μM, Sigma), Fluo-4-AM (5 μM, Invitrogen), AAV serotype 9 carrying GCaMP6 under control of the Thy1 promoter, a marker of retinal ganglion cells (AAV. GCaMP6, 10^{13} particles per ml, Penn Vector Core) or nifedipine (30 μM, Sigma). The tip of a custom-made glass micropipette was inserted into the superior quadrant of the eye at an approximately 45° angle, through the sclera into the vitreous body, avoiding injury to eye structures or retinal detachment.

Correlative focused ion-beam scanning electron microscopy (FIB-SEM)

NG2–DsRed mice were deeply anaesthetized and transcardially perfused with paraformaldehyde (2%) and glutaraldehyde (2.5%). Retinas were dissected out and incubated in lectin to visualize IP-TNTs. A two-photon microscope (LSM780, Zeiss) was used to identify a region of interest and create 3D fiducial landmarks by near infrared branding. The region of interest was further imaged by confocal microscopy (Leica Microsystems). Samples were fixed overnight in glutaraldehyde (2.5%) in sodium cacodylate buffer (0.1 M, pH 7.4), post-fixed in OsO_4 (1%) and potassium ferrocyanide (1.5%), stained with uranyl acetate (1%), dehydrated in graded ethanol solutions and embedded in Epon. Blocks were trimmed and en-face thick sections were cut with an EM ultramicrotome (UC7, Leica Microsystems) and stained with toluidine blue for imaging by light microscopy. Milling of serial sections and imaging of the block face after each *z* slice was carried out with the FEI Helios Nanolab 660 DualBeam using Auto Slice & View G3 version 1.5 software (Thermo Fisher). Distinct imaging fiducials for both ion and electron beam imaging were used to dynamically correct for drift in the *x* and *y* directions by applying appropriate SEM beam shifts. Milling was performed at 30 kV with an ion beam current of 2.5 nA, stage tilt of 9° and working distance (WD) of 4 mm. With each step, a 10-nm thickness of the material was removed by the ion beam. Each newly milled block face was then imaged with the Through-the-Lens detector for backscattered electrons at an accelerating voltage of 2 kV, beam current of 0.4 nA, stage tilt of 47° and WD of 4 mm. Pixel resolution was 10 nm with a dwell time of 30 µs. Pixel dimensions of the recorded image were 3,072 × 2,048 pixels, 872 images per sample were collected and the contrast of the images was inversed. Visualization and direct 3D volume rendering of the acquired data sets was performed with TrakEM2 by Fiji (NIH) and 3D reconstruction with Imaris software (Bitplane).

Two-photon laser scanning microscopy (TPLSM) live imaging

In vivo TPLSM retinal imaging was performed as previously described[30] with modifications. Anaesthetized mice were placed on a custom-made setup designed to accommodate light stimulation during live retinal imaging. Mice were kept on a homoeothermic blanket (Stoelting) to maintain body temperature (37 °C) during imaging. The superior and inferior eyelids were opened and a 6.0 suture, attached to the superior ocular muscle, was used to rotate the eyeball to expose the sclera atop the medial superior and peripheral retina. The conjunctiva over the sclera was gently teased to allow the placement of a 5-mm-diameter coverslip (Harvard apparatus), generating a flat plane for positioning the objective of a multiphoton microscope (LSM780, Zeiss) controlled by Zen software (Zeiss) (field of view: 400 × 400 µm). For excitation, a mode-locked Ti:sapphire laser (Chameleon Ultra, Coherent) was used through a water-immersion objective (×20, NA = 1.0, Zeiss). To track mitochondrial movement along IP-TNTs, we used mito-Dendra 2 mice (see 'Experimental animals'). Because mito-Dendra2 mice are pigmented, imaging was performed through a small scleral flap that preserved the integrity of the retina. Fluorescently tagged lectin (Thermo Fisher) or phalloidin (Biotium) was intravitreally injected 1 h before imaging for intravital visualization of IP-TNTs or F-actin, respectively. For light-triggered visual stimulation, a flash stimulus (10^2 cd m^{-2}, 5 ms) was generated with a Powerlab unit (ADInstruments), controlled by the software Labchart 8 (ADInstruments) and presented using a white-light-emitting diode, centred relative to the pupil and located 5 mm from the corneal apex. Stimulus onset ($t = 0$) and TPLSM imaging recording were synchronized offline by identifying the frame at which the light stimulus was registered. Image acquisition was carried out using a wavelength of 820 nm to excite TRICT/DsRed, FITC-dextran or Dendra2 and a mean laser power at the sample plane of 15–50 mW. Imaging was performed through the entire thickness of the retina below the sclera (depth: 50–200 µm). Multiple fields (25 × 25 µm, 90 × 90 pixels) were scanned at 12 Hz and acquired during light stimulation. Recordings with large-amplitude motion were discarded.

Ca^{2+} recordings and quantification

IP-TNTs and associated pericytes were identified by TPLSM in NG2–GCaMP6 mice after intravitreal injection of TRITC-lectin. Ca^{2+} transients in regions of interest were longitudinally recorded by TPLSM (excitation: 920 nm). Ca^{2+} signals were calculated as $\Delta F/F = (F - F_0) \times 100/F_0$, where F_0 is the fluorescence baseline and F the fluorescence at time t. Ca^{2+} transients (maximum peaks) were manually quantified with Microsoft Excel (Microsoft) when the maximum peak was ≥20% over baseline fluorescence, and their frequency calculated at each region of interest. In general, Ca^{2+} transients were defined as rapid intracellular Ca^{2+} increases in individual pericytes. Intercellular Ca^{2+} waves, which represent a subset of Ca^{2+} transients between IP-TNT-connected pericytes, were identified and recorded as synchronous Ca^{2+} peaks in both pericytes within a window of 3 s around each peak, as described[20]. To evaluate Ca^{2+} responses in retinal ganglion cells, AAV.GCaMP6 was administered by intravitreal injection 3 weeks before TPLSM imaging. Retinal ganglion cells expressing GCaMP6 were scanned at 40 Hz and Ca^{2+} signals analysed, as above, in a region of interest defined with ImageJ (NIH). Light-evoked Ca^{2+} responses were measured before and after laser exposure. For analysis of Ca^{2+} signals in endothelial cells, the Ca^{2+} indicator Fluo-4-AM (Invitrogen) was intravitreally injected 1 h before imaging. For ex vivo quantification of Ca^{2+} signals, eyes were removed and fixed in 4% PFA, and retinas were flat-mounted. Using an unbiased stereological sampling approach, as described above, images were acquired over the entire retina with identical exposure time and gain settings for all experimental and control groups (×40 objective, ApoTome 2, Zeiss). The fluorescence intensity in each cell was measured manually with ImageJ (NIH) and the background fluorescence, obtained from three square surrounding areas, was subtracted to yield the final value for each region of interest.

Analysis of vessel diameter and capillary dynamics

In vivo. Immediately before TPLSM imaging, tail vein injection of FITC-coupled dextran (70 kDa, 1 mg ml^{-1} in 100 µl, Sigma) or intraperitoneal injection of fluorescein (5% in 100 µl, Novartis Pharma) was performed to label vessels. To visualize IP-TNTs, we intravitreally injected TRITC-lectin 1 h before imaging. Diameter measurements were performed by placing a linear probe at the desired location, perpendicular to the fluorescent plane of the filled vessel, using ImageJ (NIH) and a freely available custom R routine (www.r-project.org). The fluorescence pattern for each frame was exported to R and the vascular diameter computed. Recordings with large-amplitude motion were discarded. Diameter changes after light stimulation were normalized relative to changes before stimulus presentation and were classified as positive or negative based on their dilation or constriction response, respectively. Maximum responses were calculated by averaging the global diameter change after light stimulus. Polynomial parametric functions were fitted to individual vessel responses to obtain the time to 50% peak vessel dilation/contraction.

Ex vivo. For analysis of vessel diameter on fixed flat-mounted retinas from NG2–DsRed mice, we used systematic uniform random sampling as described above. Images of all lectin-labelled microvessels within the 3D-disector frame were acquired with an Axio Imager M2 optical sectioning microscope (×40 objective, Zeiss) and analysed using ImageJ (NIH). The vessel diameter was measured at pericyte locations, as well as upstream and downstream of the same vessel segment, to estimate changes in diameter. We defined a constriction as a focal diameter reduction of at least 2 standard deviations of the mean diameter in control animals (reduction ≥35%). The total number of microvessel constrictions was calculated using the fractionator method[29], as above, and used to estimate the mean values for experimental and control groups.

Blood flow measurements

FITC-coupled dextran was administered by tail vein injection, and blood flow was assessed by quantification of red blood cells that crossed a defined location per unit time before and after light stimulation. Blood cells do not take up FITC-dextran, and hence they are identified as shadows against the fluorescent background. Capillaries from all plexuses of the retina were scanned at 40 Hz and light-evoked blood flow changes were recorded. Capillaries showing large-amplitude motion and unclear erythrocyte movement were discarded.

Laser-induced IP-TNT ablation

To ablate individual IP-TNTs in vivo, we used calibrated laser parameters (60% power, 1 s) aimed at a small area (4 µm^2) encompassing a single

IP-TNT process. To confirm that adjacent cells were not affected during IP-TNT ablation, experiments were repeated by aiming the laser directly to neighbouring retinal ganglion cells or vessels. Retinas were immediately extracted, fixed and labelled for quantification of the density of retinal ganglion cells (see below). The threshold for disruption of capillary integrity was determined using 60% laser power and a range of exposure times (1–8 s) and was visualized by leakage of intravenously delivered FITC-coupled dextran or fluorescein (332 Da) into the extracellular space.

Transient retinal ischaemia-reperfusion

Transient retinal ischaemia was performed by ligature of the ophthalmic vessels to block blood flow for up to 60 min. Under general anaesthesia, the left optic nerve was exposed and the optic nerve dural sheath was opened longitudinally. A fine (10-0) nylon suture was carefully introduced between the sheath and the optic nerve, and tied around the sheath. Because the optic nerve sheath contains the ophthalmic artery, this procedure interrupts retinal and choroidal blood flow without damaging the optic nerve itself. The ligature was released after 60 min of transient ischaemia to allow blood reperfusion to the retinal tissue. Quantitative analysis of damaged IP-TNTs was carried out in vivo by TPLSM, as described above, in fixed tissue by counting the number of DsRed- and lectin-positive ruptured processes in randomly located 3D disectors using systematic uniform random sampling and the fractionator method, as above.

Oxygen–glucose deprivation model

Retinas were collected and placed in aCSF (145 mM NaCl, 26 mM $NaHCO_3$, 1.2 mM Na_2HPO_4, 2.5 mM KCl, 1.3 mM $MgCl_2$, 2.5 mM $CaCl_2$, 10 mM glucose, pH 7.4) bubbled with 95% O_2, 5% CO_2 at 34 °C. Oxygen–glucose deprivation (simulated ischaemia) was induced by replacing glucose (10 mM) for sucrose (7 mM) and by superfusing the tissue with 95% N_2 and 5% CO_2 to deplete oxygen. Retinal explants were incubated in these conditions for a total of 45–60 min and then analysis of IP-TNT-coupled pericytes was performed.

Laser-induced focalized retinal ischaemia

To induce focalized ischaemia in retinal microregions, deeply anaesthetized mice received a tail vein injection of Rose bengal (8 mg ml^{-1}, Sigma), a photosensitive dye that induces capillary clotting upon laser-induced activation[25]. A laser spot was applied to a single capillary (532 nm, Chameleon Ultra, Coherent) at 50 mW power (duration: 5 s, spot size: 3 µm) to induce focal ischaemia. A maximum of 10 capillaries per retina were photocoagulated. Capillary occlusions were highly reproducible and could be targeted to specific locations. This procedure creates an ischaemic microregion of 150–200 µm in diameter, thus allowing high-quality TPLSM imaging of ischaemic versus non-ischaemic regions in the same retina. IP-TNTs were quantified in consecutive areas centred on the photocoagulated capillary spot with an increasing-radius step of 50 µm. The light-evoked capillary responses in each ischaemic microregion was recorded immediately after single-capillary photocoagulation. Non-ischaemic microregions in the same retina, located at least 600 µm away from the photocoagulation site, were analysed as controls.

Quantification of retinal ganglion cell and pericyte densities

NG2–DsRed retinas were incubated with RBPMS (PhosphoSolutions), a specific marker of retinal ganglion cells, and then rinsed, mounted vitreal side up, covered with anti-fade solution (SlowFade, Molecular Probes) and visualized by fluorescence microscopy as described. Using the stereological random sampling method described above, RBPMS-labelled retinal ganglion cells and DsRed-positive pericytes were counted using 3D disectors (stacks) throughout the entire retina, and the total number of retinal ganglion cells or pericytes was calculated using the fractionator method[29].

Statistical analyses

Data analysis was always carried out with blinding by third-party concealment of treatment using uniquely coded samples. For all the experiments carried out in this study, we used an unbiased stereological approach based on systematic random sampling both ex vivo and in vivo. This approach, described in detail above, involved randomly placing 3D-disectors (stacks) across the entire retina for ex vivo experiments, or the entire retinal area imaged with the multiphoton microscope for in vivo experiments. This approach ensured that our data was collected randomly from a large population available for analysis, therefore avoiding bias. The number of animals used in each experiment as well as the number of structures (IP-TNTs, capillaries and pericytes) analysed are indicated in the figure legends. An appropriate sample size was determined by power calculation when the study was designed. For sample size estimates, power calculations were used to determine the number of animals required per group for any given experiment to achieve an 80% power to detect a statistically significant difference at $\alpha = 0.05$. The detailed number of animals used in each group as well as the number of IP-TNTs and capillaries analysed are indicated in the figure legends. Details of randomization and choice of sample predetermination can also be found in the Reporting Summary. All values are provided as the mean ± standard error of the mean (s.e.m.), and individual values are presented in each graph. Statistical analysis was performed with Prism 7 (GraphPad). We evaluated all cohorts with normality (Shapiro–Wilk test) and variance (*F*-test) tests. Values corresponding to response time, vessel diameter, blood flow, number of constrictions, intracellular Ca^{+2} and stereological quantifications were compared by means of two-tailed Student's *t*-test or Mann–Whitney *U* test, where appropriate. For multiple comparisons, we used analysis of variance (ANOVA) followed by Dunnett's or Tukey's test, where appropriate. A *P* value ≤ 0.05 was considered significant. All regression lines of diameter change graphs were fit with the same order between experimental and control cohorts.

Reporting summary

Further information on research design is available in the Nature Research Reporting Summary linked to this paper.

Data availability

All the data analysed in this study, including raw data, are provided in this published article and the supplementary information files. There are no restrictions on data availability. Source data are provided with this paper.

Code availability

The R code used for data analysis is included in the Supplementary Information files.

29. Mouton, P. R. *Principles and Practices of Unbiased Stereology: An Introduction for Bioscientists* (Johns Hopkins Univ. Press, Baltimore, 2002).
30. Takihara, Y. et al. In vivo imaging of axonal transport of mitochondria in the diseased and aged mammalian CNS. *Proc. Natl Acad. Sci. USA* **112**, 10515–10520 (2015).

Acknowledgements We thank T. Kennedy, N. Belforte, P. D'Onofrio, Y. Shiga, and R. Araya for comments on the manuscript; J. Mui and W. Leelapornpisit for assistance with sample preparation, microscope operation and data collection; and G. Seifert and C. Steinhäuser for providing eyes from CX43–ECFP mice. Supported by grants from the Canadian Institutes of Health Research (A.D.P.).

Author contributions L.A.-M. conceived the hypothesis and the study design, established the method for intravital imaging of the retina; performed surgeries, in vivo experiments, stereological analysis and 3D reconstruction; collected images and data; programmed analysis software; analysed the data; prepared figures and videos; contributed to the design and development of transgenic animals; and wrote the paper. D.V.-B. performed single-pericyte electroporation, in vivo, ex vivo and FIB-SEM experiments, microsurgeries to induce retinal ischemia and reperfusion, and immunohistochemistry for image acquisition and 3D reconstruction; collected images and data; performed stereological analysis; prepared figures and videos; and wrote the paper. H.Q. performed immunohistochemistry for 3D reconstruction, collected images, performed quantification and analysis of IP-TNTs, and prepared figures. J.B.K. participated in the FIB-SEM experiments and data analysis. F.D. performed breeding and production of all mice as well as genotyping and colony maintenance, and contributed to data analysis. K.K.M. contributed to experimental design, FIB-SEM experiments and data analysis. A.P. participated in imaging experiments, data analysis and writing of the paper. P.D. performed ex vivo experiments and participated in data analysis and writing of the paper. A.D.P. conceived the hypotheses, designed and supervised the study, contributed to data analysis, acquired funds and administered the project, and wrote and edited the paper. All authors contributed to the discussion of the results and writing of the paper.

Competing interests The authors declare no competing interests.

Additional information

Supplementary information is available for this paper at https://doi.org/10.1038/s41586-020-2589-x.

Correspondence and requests for materials should be addressed to L.A.-M. or A.D.P.

Peer review information *Nature* thanks Mark Nelson, Frank Winkler, Chiara Zurzolo and the other, anonymous, reviewer(s) for their contribution to the peer review of this work.

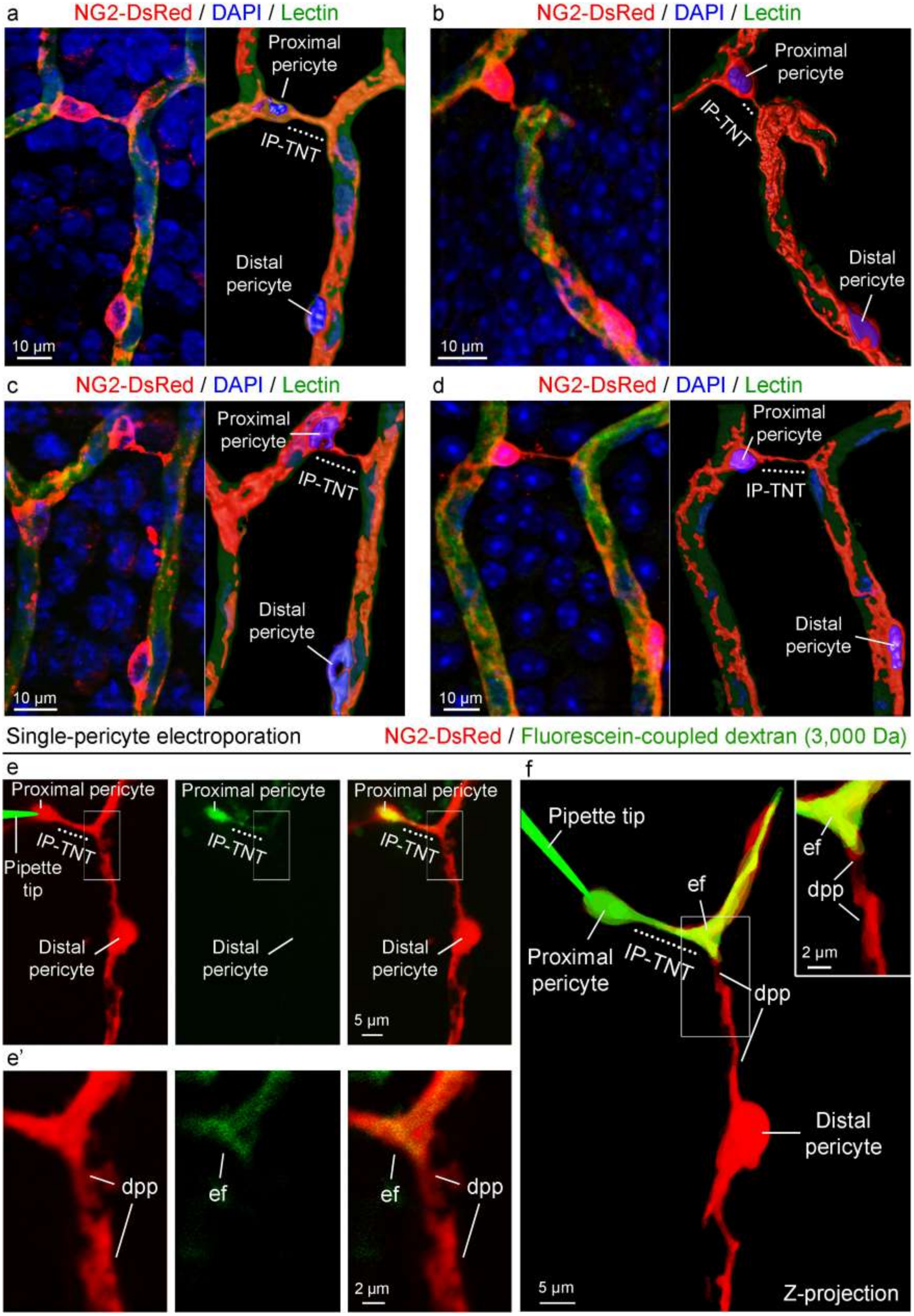

Extended Data Fig. 1 | IP-TNTs connect two bona fide pericytes located on separate capillaries. a–d, Representative examples of NG2–DsRed retinas labelled with DAPI (blue) and lectin (green) in combination with 3D reconstruction (right panel for each set) showing a pericyte and its IP-TNT (dotted line), termed here the proximal pericyte, connecting with the processes of a pericyte located on a distal capillary (distal pericyte). IP-TNTs connected a proximal pericyte with a distal one in all retinas analysed. Pericytes and their processes are shown in red. **e**, Single-pericyte electroporation of fluorescein-coupled dextran (3,000 Da) into a DsRed-positive pericyte with an IP-TNT (dotted line). Dextran entered the proximal pericyte (green) and IP-TNT but did not diffuse into the distal pericyte (red), allowing clear identification of the two connected pericytes. **e′**, Higher-magnification inset shows the interface between the two IP-TNT-coupled pericytes at the level of the IP-TNT end-foot (ef, green) and the distal pericyte process (dpp, red). **f**, 3D reconstruction unambiguously shows that the two pericytes are in contact at the level of the IP-TNT end-foot and distal pericyte process. Experiments were replicated 4 times.

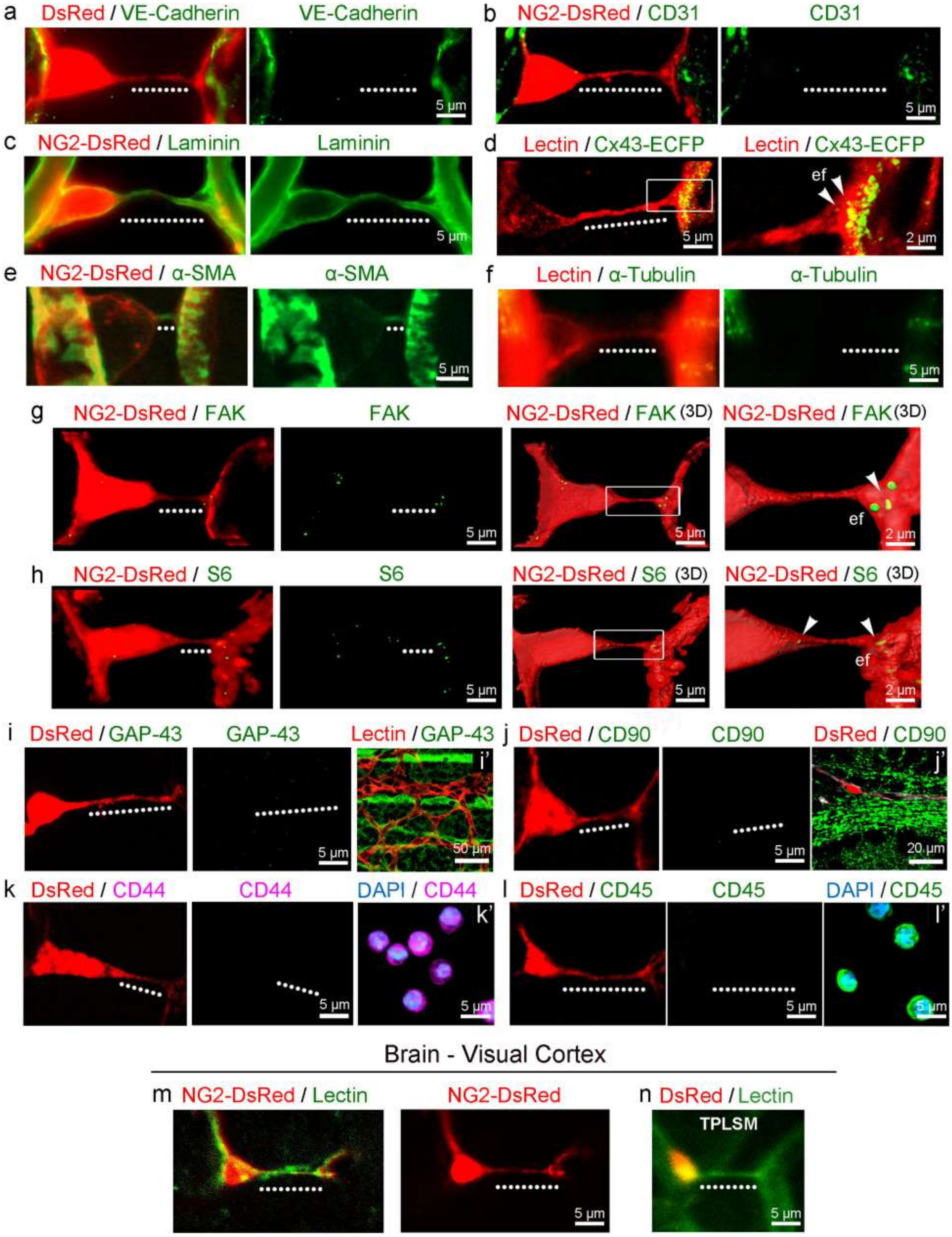

Extended Data Fig. 2 | IP-TNT characterization: localization of molecular markers and presence in the brain. **a**, **b**, NG2–DsRed and lectin-labelled IP-TNTs (dotted line) show absence of immunolabelling for the endothelial cell markers VE-cadherin and CD31. **c**, Labelling for the basal lamina component laminin confirmed that IP-TNTs are enclosed by a basement membrane. **d**–**f**, Representative IP-TNT from CX43–ECFP reporter mouse retina showing endogenous CX43 expression in the IP-TNT end-foot (ef; **d**). IP-TNTs contain the contractile protein α-SMA (**e**), but not α-tubulin (**f**). **g**, **h**, Immunolabelling and 3D reconstruction demonstrated that FAK and S6 proteins are localized in IP-TNTs, notably at end-feet (arrowheads). **i**–**l**, IP-TNTs do not contain either GAP43 or the mesenchymal stem cell markers CD90, CD44 or CD45. Positive controls for each antibody were postnatal day 5 retinal ganglion cell axons for GAP43 (**i'**), retinal ganglion cells for CD90 (**j'**) and peripheral leukocytes for CD44 (**k'**) and CD45 (**l'**). **m**, **n**, IP-TNTs detected in the visual cortex shown in fixed tissue (**m**) and by TPLSM in vivo (**n**). A minimum of 100 IP-TNT-connected pericytes from 5 different animals were analysed for each marker.

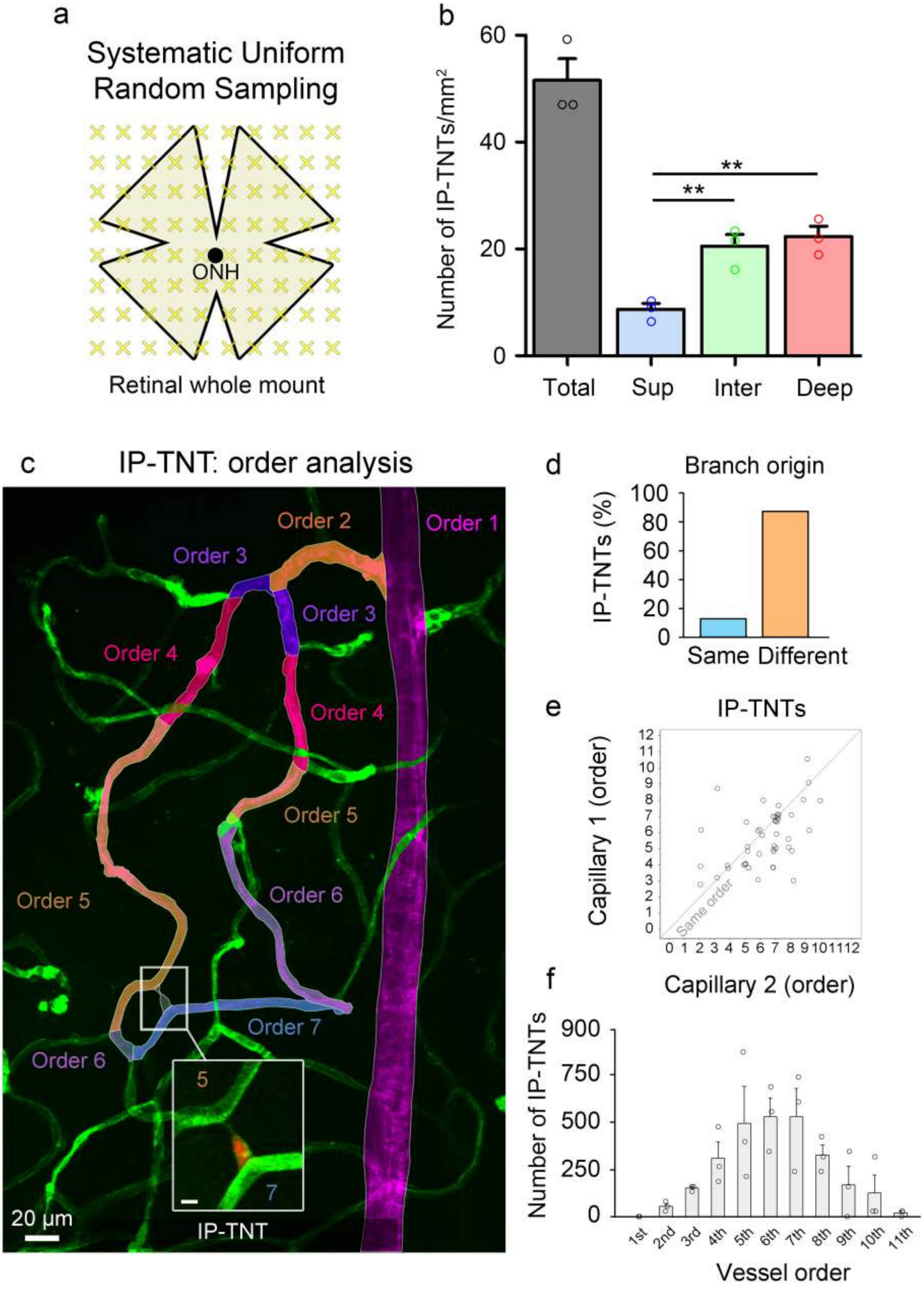

Extended Data Fig. 3 | IP-TNTs exist in all retinal vasculature plexuses and connect distal capillaries of the same and different orders. **a**, Schematic of the systematic uniform random sampling method used for histological quantification in whole-mounted retinas. **b**, Quantitative analysis demonstrated that IP-TNTs are abundant in all plexuses of the retinal vasculature, with a higher density in the intermediate and deep plexuses than in the superficial plexus ($n = 3$ mice, two-tailed ANOVA Tukey's test, $^{***}P < 0.001$). **c**, 3D reconstruction of a representative vascular network in which each branch order has been pseudocoloured. The first-order vessel was defined as the first branch division (arteriole) from the central retinal artery, and subsequent branches were assigned consecutively higher orders ($n = 3$ mice). **d**, Most IP-TNT-linked capillaries (87%) originate from different branches (87%), while the remainder derive from the same branch ($n = 94$ IP-TNTs/capillaries, $n = 3$ mice). **e**, IP-TNTs connected pericytes located either on same-order vessels (values on diagonal line) or different-order vessels (values above or below diagonal line) ($n = 94$ IP-TNTs/capillaries, $n = 3$ mice). **f**, Analysis of the number of IP-TNTs per vessel order shows that these processes are more prevalent in fourth- to eighth-order vessels ($n = 3$ mice). Total sampled area = 560 µm × 451 µm × 10 disectors = 2,525,600 µm^2. Data are presented as mean values ± s.e.m.

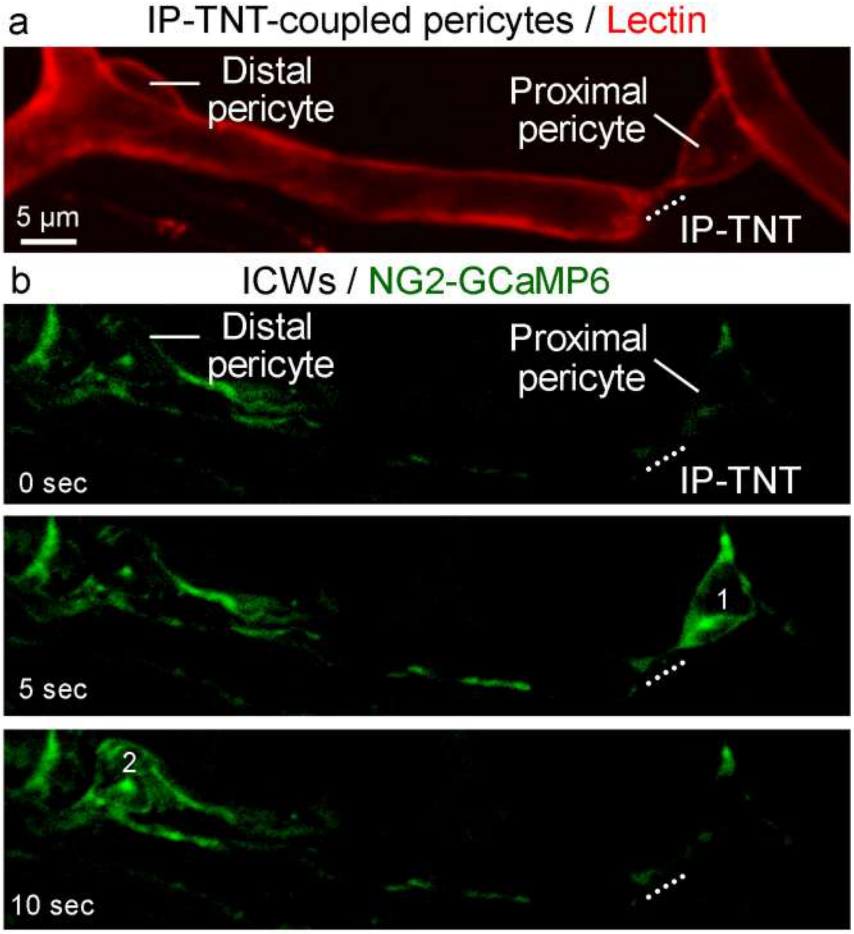

Extended Data Fig. 4 | IP-TNT-coupled pericytes communicate through intercellular Ca^{2+} waves (ICWs). **a**, **b**, Time-lapse recordings of ICWs propagation between a proximal and a distal pericyte, visualized with lectin, connected by an IP-TNT (dotted line) in NG2–GCaMP6 retinas. Panels in **b** show the propagation of ICWs over time from the proximal pericyte (1), through the IP-TNT, onto the distal pericyte (2). See Supplementary Video 3. Experiments were replicated 5 times.

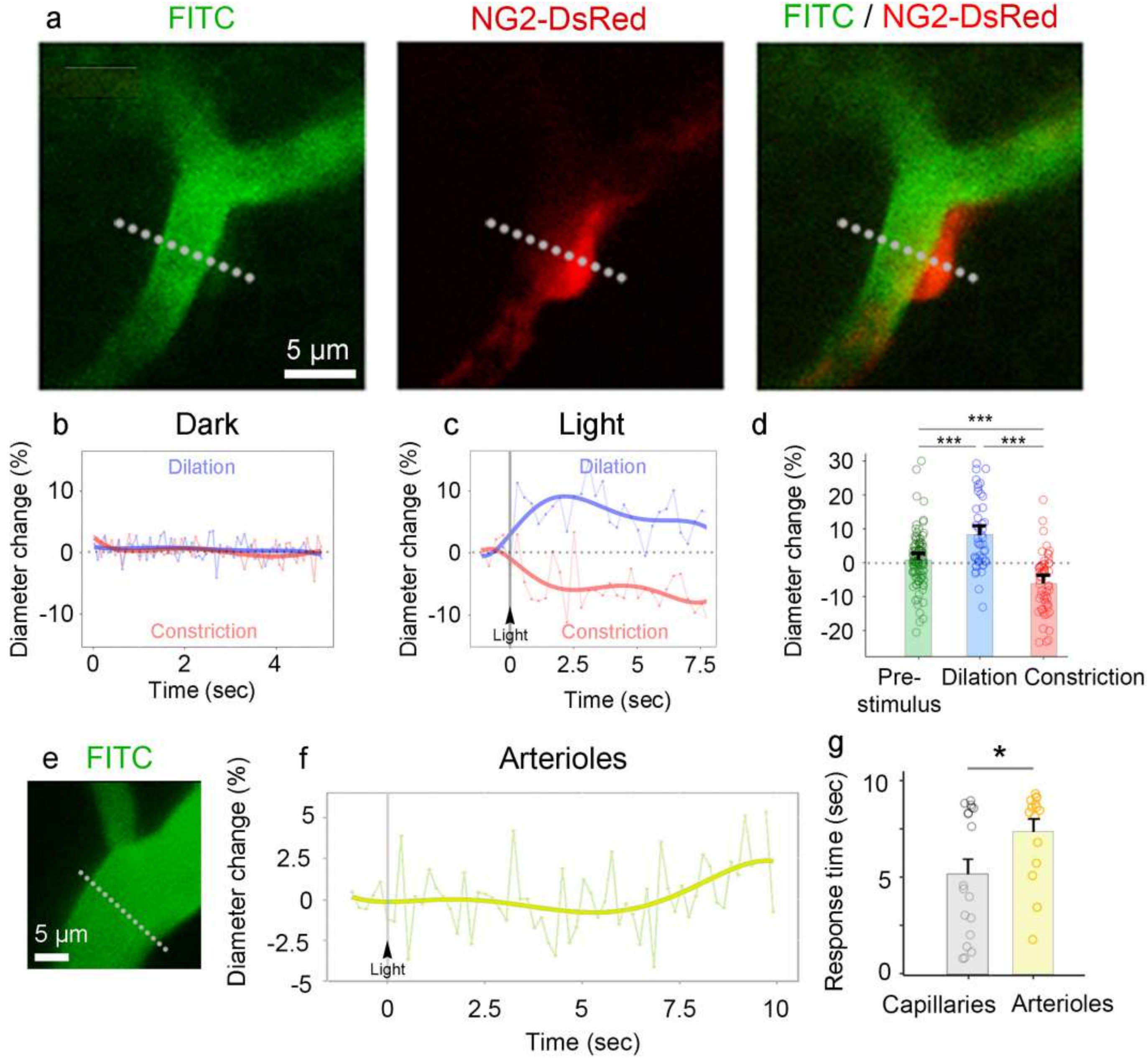

Extended Data Fig. 5 | Live TPLSM imaging of light-evoked haemodynamic responses of retinal capillaries. a, TPLSM recordings of capillary diameter changes at pericyte soma in NG2–DsRed mice subjected to a flash light stimulus (10^2 cd m^{-2}, 5 ms). A linear probe perpendicular to the capillary at a pericyte location denotes the site where capillary diameter was measured (dotted line). Experiments were replicated in 211 capillaries, $n = 4$ mice. **b**, Longitudinal analysis of diameter changes by TPLSM in vivo shows little change in capillary diameter before light stimulation (dilation: $n = 20$ capillaries, $n = 4$ mice; constriction: $n = 18$ capillaries, $n = 4$ mice). **c**, By contrast, light provoked coordinated capillary dilation (blue: $n = 46$ capillaries, $n = 4$ mice) and constriction (red: $n = 60$ capillaries, $n = 4$ mice). **d**, Maximum response graph confirms substantial light-evoked capillary dilation and constriction after a flash light stimulus (pre-stimulus: $n = 105$ capillaries, $n = 4$ mice; dilation: $n = 46$ capillaries, $n = 4$ mice; constriction: $n = 60$ capillaries, $n = 4$ mice; two-tailed ANOVA Tukey's test, $^{***}P < 0.001$). **e**–**g**, The overall response of arterioles (labelled with FITC in **e**), identified by a diameter larger than 9 µm, was substantially slower than that of capillaries (arterioles: $n = 15$ vessels, $n = 3$ mice; capillaries: $n = 18$ vessels, $n = 3$ mice; two-tailed Mann–Whitney U test, $^{*}P = 0.026$). Data are presented as mean values ± s.e.m.

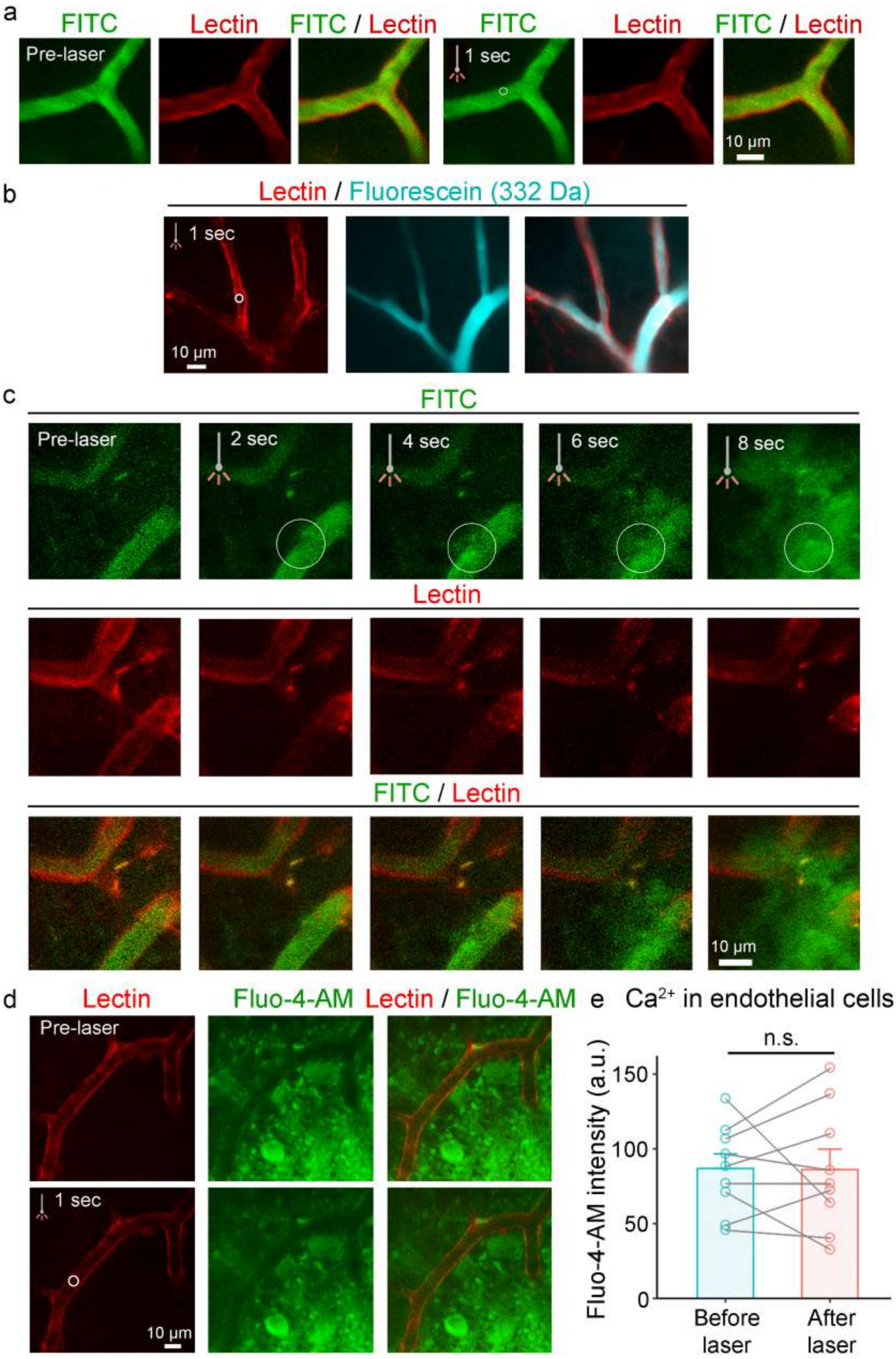

Extended Data Fig. 6 | Laser ablation does not damage endothelial cells. **a**, **b**, The laser parameters used to ablate IP-TNTs did not damage endothelial cells, even when aimed directly at capillaries, or alter blood retinal barrier integrity, as there was no leakage of FITC-coupled dextran (70 kDa, **a**) or fluorescein (332 Da, **b**). Experiments were replicated 3 times. **c**, Longer laser exposure time directed at endothelial cells in a single capillary (white circle) was required to cause damage (>4 s), as assessed by leakage of FITC-coupled dextran. Experiments were replicated 3 times. **d**, **e**, Ca^{2+} signals in endothelial cells after laser ablation, visualized with Fluo-4-AM, were indistinguishable from those in non-laser-ablated controls, suggesting that this procedure caused no major alterations ($n = 9$ capillaries per group, $n = 2$ mice per group; two-tailed Student's *t*-test, n.s., not significant). Data are presented as mean values ± s.e.m.

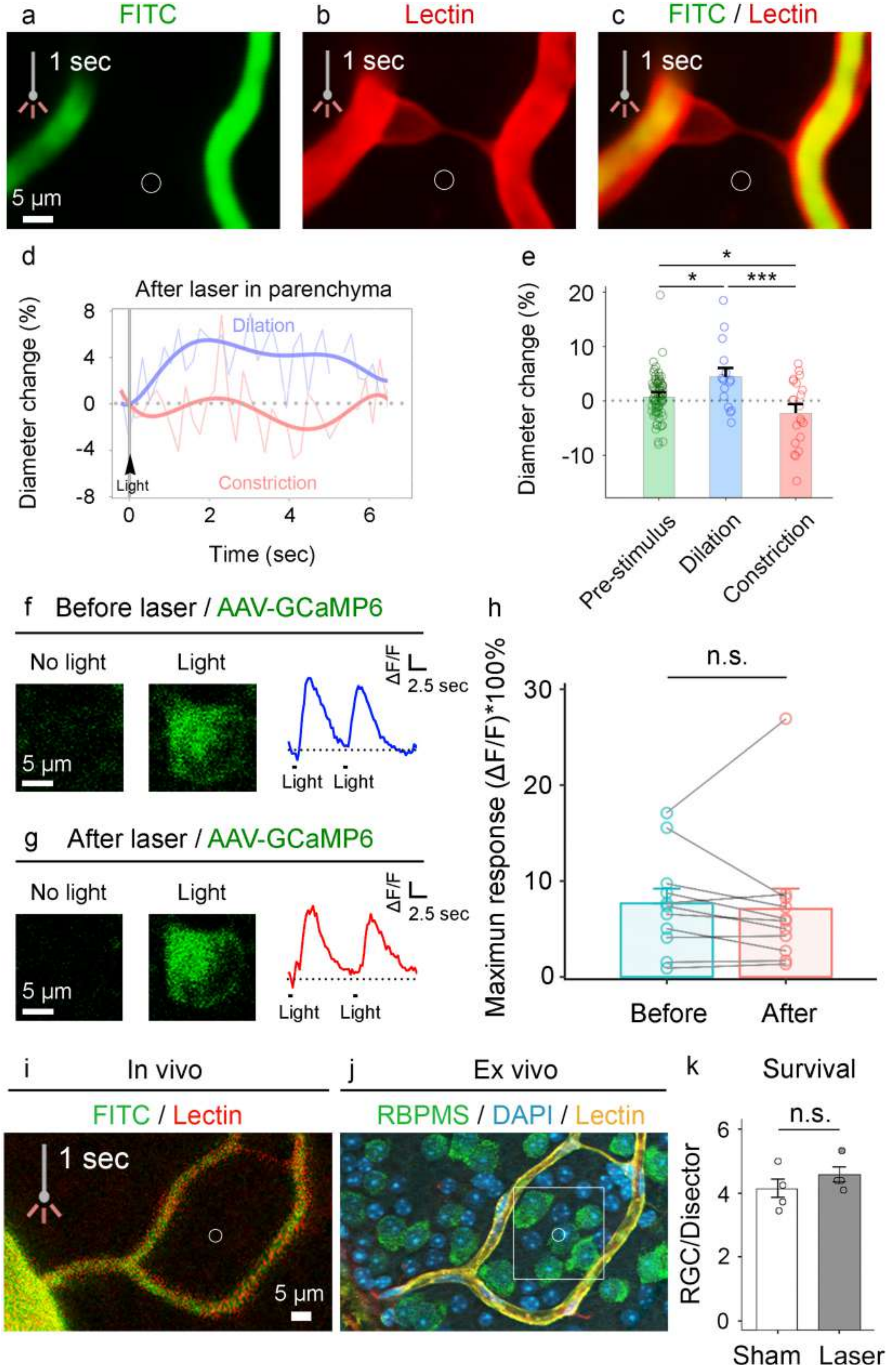

Extended Data Fig. 7 | See next page for caption.

Extended Data Fig. 7 | Laser ablation does not cause retinal neuron damage. a–**c**, The same laser parameters used to ablate IP-TNTs were applied to adjacent retinal ganglion cells (white circle). Experiments were replicated in 18 laser spots, $n = 3$ mice. **d**, **e**, Longitudinal analysis of light-evoked capillary dilation (blue; $n = 15$ capillaries, $n = 3$ mice) and constriction (red; $n = 21$ capillaries, $n = 3$ mice) demonstrated that microvessel dynamics were preserved under these conditions (pre-stimulus: $n = 79$ capillaries, $n = 3$ mice; dilation: $n = 15$ capillaries, $n = 3$ mice; constriction: $n = 21$ capillaries, $n = 3$ mice; two-tailed ANOVA Tukey's test, $^*P < 0.05$, $^{***}P < 0.001$). **f**–**h**, An AAV was used to selectively express GCaMP6 in retinal ganglion cells and monitor their ability to respond to light following laser ablation. Identical light-evoked Ca^{2+} responses were recorded before and after laser exposure, confirming the functional integrity of these neurons ($n = 11$ retinal ganglion cells per group, $n = 3$ mice per group; two-tailed Student's *t*-test, n.s., not significant). **i**, **j**, Retinas were extracted after the experiment and immunostained with an antibody against RBPMS (specific for retinal ganglion cells), and neuronal density was analysed at the site of laser application (white circle within square). Experiments were replicated in 39 laser spots, $n = 4$ mice. **k**, Quantification of retinal ganglion cell numbers across a 2,000-μm^2 disector area centred at the laser site revealed no significant difference in neuronal density relative to equivalent non-lasered areas ($n = 43$ control disectors, $n = 39$ laser-treated disectors, $n = 4$ mice per group; two-tailed Student's *t*-test, n.s., not significant). Data are presented as mean values ± s.e.m.

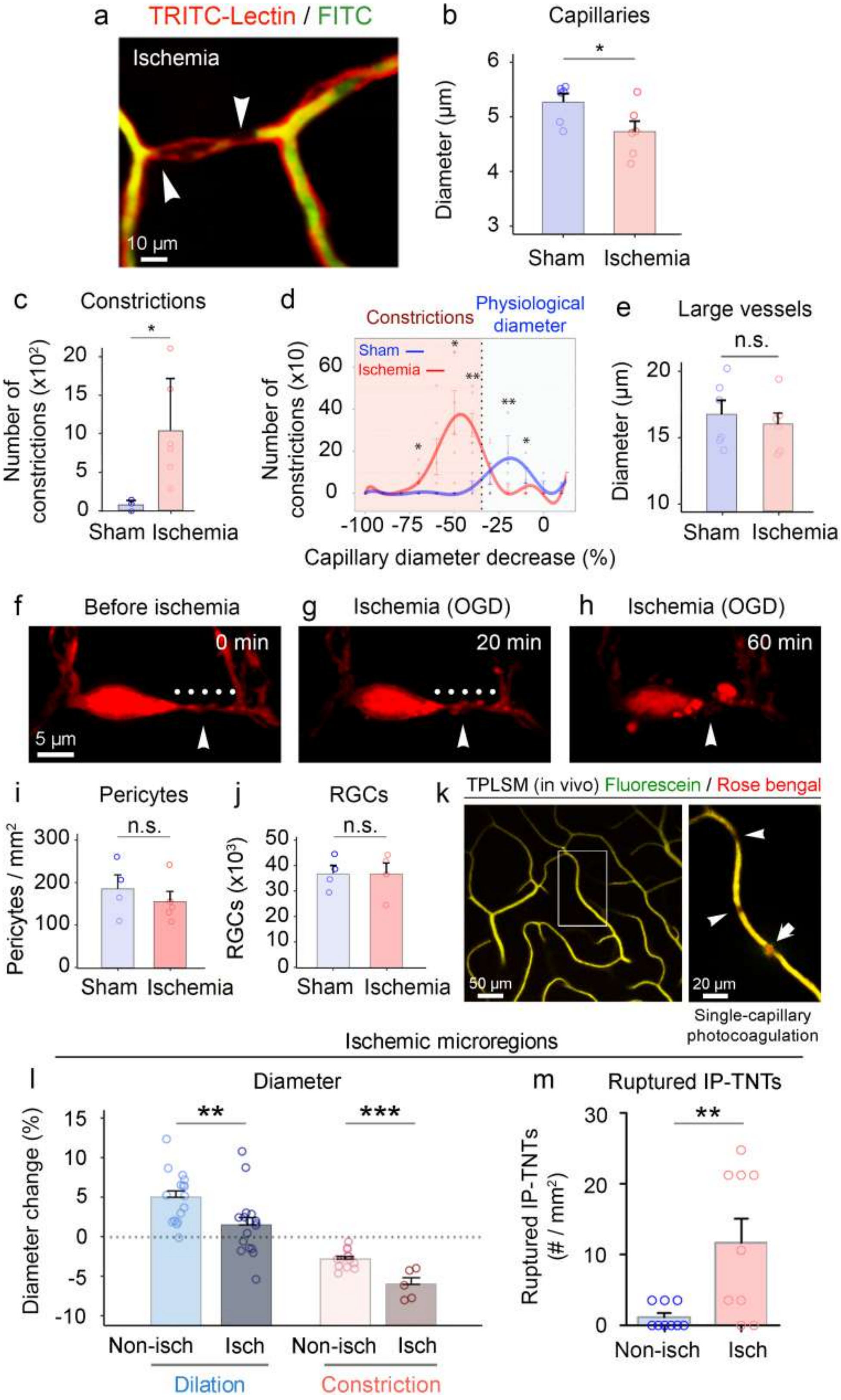

Extended Data Fig. 8 | See next page for caption.

Extended Data Fig. 8 | Ischaemia leads to pericyte-mediated capillary constriction and IP-TNT rupture. a, In vivo TPLSM imaging of TRITC-lectin-labelled ischaemic retina, showing constricted capillary sites at pericyte locations (arrowheads). Experiments were replicated 3 times.

b, **c**, Quantification of capillary diameter (**b**; $n = 6$ mice per group; two-tailed Student's *t*-test, $^*P = 0.049$) and number of constrictions (**c**; sham: $n = 4$ mice; ischaemia: $n = 6$; two-tailed Student's *t*-test, $^*P = 0.023$) in whole-mounted ischaemic and sham-operated control retinas. **d**, Frequency distribution of the number of constrictions relative to the degree of decrease in capillary diameter (%) in sham-operated controls (blue trace) and ischaemic retinas (red trace) (sham: $n = 4$ mice; ischaemia: $n = 6$; two-tailed Student's *t*-test, −70% $^*P = 0.013$, −50% $^*P = 0.019$, −40% $^{**}P = 0.004$, −20% $^{**}P = 0.005$, −10% $^*P = 0.048$).

e, Changes in diameter of large vessels in ischaemic and sham-operated whole-mounted retinas ($n = 6$ mice per group, two-tailed Student's *t*-test, n.s., not significant). **f**–**h**, Analysis of IP-TNTs in NG2–DsRed retinas before and after oxygen–glucose deprivation (OGD), to mimic ischaemia ex vivo. Arrowheads point at an intact IP-TNT before damage (**f**) and to the rupture of the process after 20 and 60 min of ischaemia with extravasation of DsRed into the extracellular space (**g**, **h**). Experiments were replicated 5 times.

i, **j**, Quantification of the numbers of pericytes, visualized in Ds-Red retinas (**i**; sham: $n = 4$ mice; ischaemia: $n = 5$; two-tailed Student's *t*-test, n.s., not significant), and retinal ganglion cells, visualized with the retinal ganglion cell marker RBPMS (**j**; $n = 4$ mice per group; two-tailed Student's *t*-test, n.s., not significant), showed that these cells do not die in ischaemic retinas (1 h ischaemia) relative to sham-operated controls. **k**, Induction of ischaemic retinal microregions after tail vein injection of Rose bengal by application of a laser to a single capillary (arrow in inset), which causes blood cells to stall in photocoagulated capillaries (arrowheads in inset). Experiments were replicated in 17 laser spots; $n = 7$ mice. **l**, Light-evoked capillary responses were substantially reduced in ischaemic retinal microregions induced by Rose bengal photocoagulation (dilation: sham, $n = 16$ capillaries, $n = 4$ mice, reperfusion, $n = 17$ capillaries, $n = 4$ mice; constriction: sham, $n = 13$ capillaries, $n = 4$ mice, reperfusion, $n = 5$ capillaries, $n = 4$ mice; two-tailed Student's *t*-test, $^{**}P = 0.009$, $^{***}P < 0.001$). **m**, Quantitative analysis confirmed a substantial loss of IP-TNTs in ischaemic versus non-ischaemic microregions within the same retina ($n = 9$ microregions per group, $n = 3$ mice per group; two-tailed Student's *t*-test, $^{**}P = 0.008$). Data are presented as mean values ± s.e.m.

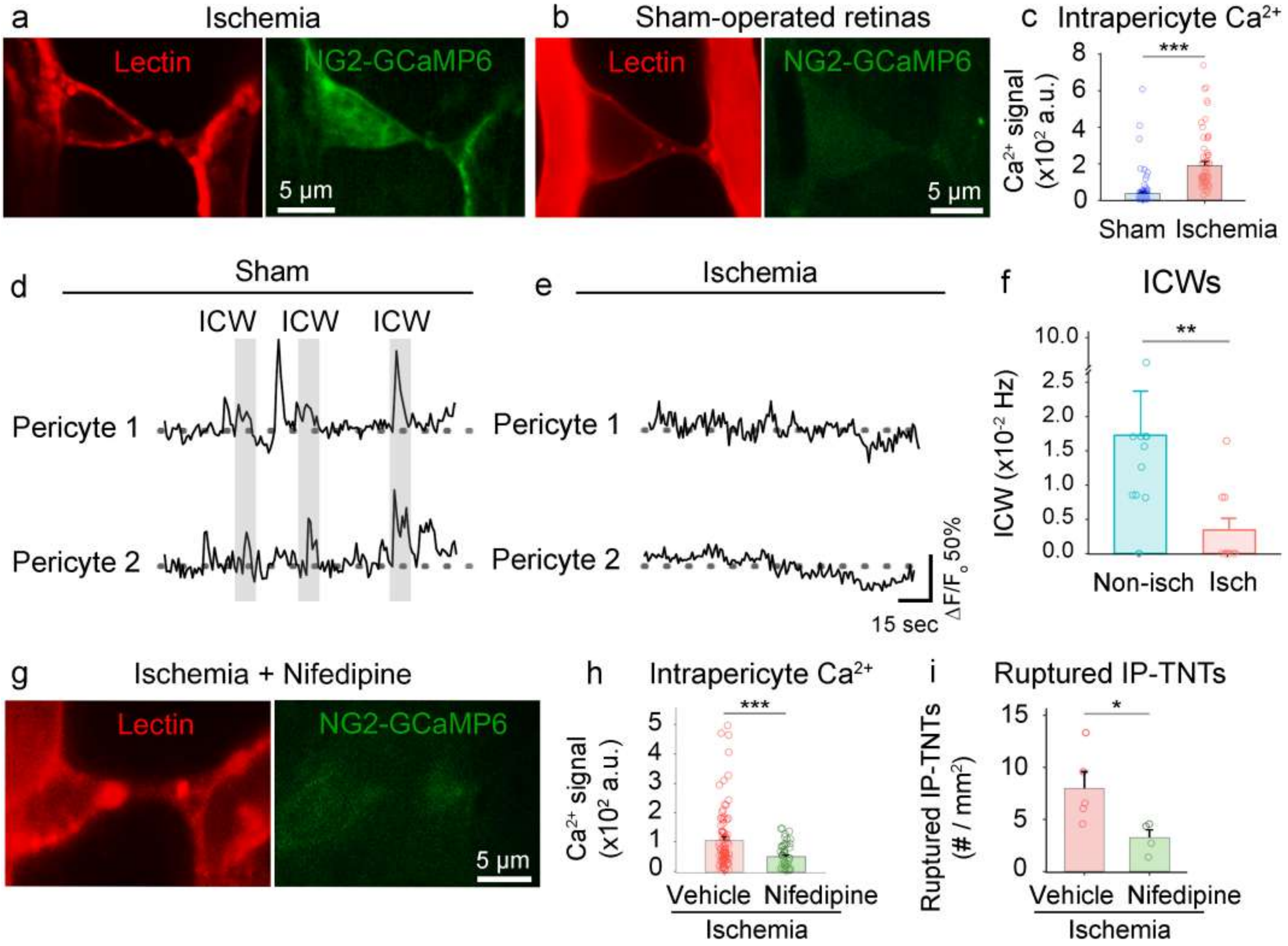

Extended Data Fig. 9 | Ca^{2+} influx during ischaemia disrupts IP-TNT-mediated ICWs, and the Ca^{2+} blocker nifedipine protects IP-TNTs. **a**–**c**, Imaging of NG2–GCaMP6 mouse retinas showed that transient retinal ischaemia triggered a significant increase in intracellular Ca^{2+} in pericytes and their IP-TNTs relative to those in sham-operated controls (sham: $n = 114$ pericytes/IP-TNTs, $n = 3$ mice; ischaemia: $n = 70$ pericytes/IP-TNTs, $n = 3$ mice, two-tailed Mann–Whitney U test, $^{***}P < 0.001$). **d**–**f**, The frequency of ICWs between IP-TNT-coupled pericytes was markedly reduced in ischaemic retinas relative to sham controls (in **f**, sham: $n = 24$ capillaries, $n = 4$ mice; ischaemia: $n = 20$ capillaries, $n = 4$ mice; two-tailed Mann–Whitney U test, $^{**}P = 0.007$). **g**–**i**, A single intraocular injection of the Ca^{2+} channel blocker nifedipine (30 μM), before ischaemia, was sufficient to lower intrapericyte Ca^{2+} (**g**, **h**; in **h**, vehicle: $n = 90$ pericytes, $n = 4$ mice; nifedipine: $n = 49$ pericytes, $n = 4$ mice; two-tailed Mann–Whitney U test, $^{***}P < 0.001$) and reduce the number of ruptured IP-TNTs (vehicle: $n = 5$ mice; nifedipine: $n = 4$ mice; two-tailed Student's t-test, $^{*}P = 0.039$; **i**). Data are presented as mean values ± s.e.m.